2023-04-01

Analyzing drainage basin orientation and its relationship to active fold growth (Handun anticline, Zagros, Iran)

Bahrami, S

10.1016/j.geomorph.2023.108605
Geomorphology
Elsevier

Analyzing drainage basin orientation and its relationship to active fold growth (Handun anticline, Zagros, Iran)

Shahram Bahrami[1], Martin Stokes[2]

1- Department of Physical Geography, School of Earth Sciences, Shahid Beheshti University, Tehran, Iran

2- School of Geography, Earth and Environmental Sciences, University of Plymouth, Plymouth, UK

Abstract

Combinations of tectonic geomorphological criteria are frequently used to detect vertical and lateral growth of fold structures in tectonically active settings due to their low cost and relative ease of application. The purpose of this study is to analyze the morphometric properties of drainage basins developed into the flanks of a growing anticline to explore the active tectonic growth patterns of the fold. We target the Handun anticline in the Zagros Simply Folded Belt due to it being actively growing fold structure and that possesses a high variability of drainage basin morphologies across different parts of the fold structure.

57 drainage basins were characterized in terms of their orientation using a newly defined drainage basin orientation (DBO) index, in combination with a set of standard tectonic geomorphological metrics (drainage basin area [Ba], slope [S], asymmetry factor [AF], hypsometric integral [HI], basin shape [Bs], crescentness index [CI], sinuosity of main drainage [Smd], drainage density [Dd], drainage density of 1st-order streams [Dd1], drainage frequency [Df]) and sinuosity of the main anticline ridge [Sad]). Indices were synthesized for spatial comparison between western, central and eastern zones of the growing fold.

Results show that the DBO is strongly correlated with its CI, Smd, and A. In terms of spatial distribution, the central zone (the main fold axis) is characterized by lower values of DBO, A, S, CI, Smd, and Sad. These contrast with the western and eastern zones (fold plunge regions),

which are characterized by higher values of Dd, Dd1, and Df. Of note is the southern limb of the anticline, which is characterized by drainage basins with larger A, and higher values of AF, CI, and Smd. This suggests higher lateral erosion on the southern fold flanks. In contrast, drainage basins with steeper S, and greater DBO elongation are found on the northern limb, suggesting dominance of vertical erosion. This contrasting south-north erosion pattern suggests that the northern fold flank is actively steepening, and presenting a more youthful topography, with lower and spatially focused erosion that is increasing with time. Overall, high values of the newly proposed DBO metric relate to the presence of a curved and / or an asymmetric forked drainage pattern that is configured to the trend of faults and fractures across the fold. These structures are typically oriented oblique to the fold axis, with further modification into a semi-annular drainage pattern developed around a salt diapir.

Keywords: Drainage basin orientation, tectonic geomorphological indices, folds, anticlines

Introduction

Quantitative analysis of landforms in tectonically active regions, especially within collisional zones of elevated compressive strain, can provide useful information concerning the patterns and rates of tectonic activities and the landscape development (Jackson et al., 1998; Delcaillau et al., 2006; Ramsey et al., 2008; Keller and DeVecchio, 2022). Such analysis can be achieved through application of geomorphic indices to the landscape and its component landforms. These DEM and satellite images derived indices are low-cost, with relatively easy-to-perform data collection and analysis steps. Thus, they are highly effective tools to apply and inform on improving our understanding of active tectonics. Morphometric parameters related to drainage basins (i.e., hypsometric integral, asymmetry, elongation, circularity, crescentness index), river

networks (i.e., drainage density, frequency, confluence angle, hierarchal anomaly index), and mountain fronts (i.e., mountain front sinuosity, facet slope-to-height ratio, percentage faceting, valley floor width-to-height ratio) have been commonly applied to landscapes affected by varying tectonic activity worldwide (Wells et al., 1988; Ramírez-Herrera, 1998; El Hamdouni et al., 2008; Peréz-Peña et al., 2010; Altin and Altin, 2011; Özkaymak and Sözbilir, 2012; Bahrami, 2013; Bahrami et al., 2020; García-Delgado and Velandia, 2020; Różycka and Migoń, 2021; Bahrami, 2022). In compressional tectonic settings, the geomorphic signatures of a laterally growing (widening) fold typically includes: (1) decreases in drainage density and degree of dissection; (2) decrease in elevation of wind gaps; (3) decrease in relief along a fold topographic profile; (4) development of asymmetric drainage patterns; (5) deformation of progressively younger deposits or landforms; (6) decrease in rotation and inclination of the anticline forelimb; (7) development of an asymmetric forked tributary network; (8) development of a series of curved wind gaps; and (9) the development of fan-shaped tributary drainage patterns on fold flanks, have all been analyzed in folded structures (Keller et al., 1999; Ramsey et al., 2008; Bretis et al., 2011; Keller and DeVecchio, 2013; Collignon et al., 2015, 2016;Sissakian et al., 2019; Machuca et al., 2021; Adeoti and Webb, 2022). Nevertheless, little attention has been devoted to the drainage basin orientation and its relation to active tectonics in growing folds. The few existing studies include Ramsey et al. (2007) who evaluated the deflection of rivers using the angle between the general trend of the basin outlet with respect to an east-west direction. They suggested that deflections of rivers are controlled by the fault lines. A further example is by Krystopowicz et al. (2020) who defined a morphometric factor, called the catchment-fault azimuth, expressed as the angle between the fault and the main axis of the catchment measured in a counterclockwise direction. Their study revealed that values of basin asymmetry and basin-fault azimuth illustrate tilting of fault block footwall catchments as part of a regional tilting pattern. Generally, the trunk drainage of a basin is oriented

perpendicular to the mountain front line, whereas it is oriented oblique to the mountain front line, or fold axis, when it is affected by a fault trace or lateral growth of a fold. Thus, quantitative evaluation of the orientation of drainage basins developed on the fold flanks can obtain useful information about active tectonics.

The Zagros Simply Folded belt is one of the most tectonically active areas in the world, containing pronounced 'whaleback' anticlines that are growing vertically and laterally (Lee and Falcon, 1952; Berberian, 1995; Ramsey et al., 2008; Bahrami, 2013; Faghih and Nourbakhsh, 2014; Collignon et al., 2016; Woodbridge et al., 2019; Bahrami, 2022). Although drainage system development and morphometry have been studied as evidence of fold growth throughout the Zagros (Ramsey et al., 2008; Bretis et al., 2011; Bahrami, 2013; Collignon et al., 2016; Woodbridge et al., 2019; Bahrami et al., 2020), drainage basin orientation in association with vertical and lateral growth of folds is a less evaluated aspect. Recently, Bahrami et al. (2020) proposed a "crescentness index" of a drainage basin as a new morphometric index suggesting lateral growth of the Gorm anticline (Fars region). The study showed that the development of crescent-shaped basins in the pre-nose fold segment, where the upstream drainage basin parts have been curved towards the central region of the anticline, provides strong geomorphic evidence for lateral fold propagation. In terms of the Handun anticline which forms the focus of this study, Ramsey et al. (2008) briefly examined the effect of some oblique fractures on the orientation and pattern of its drainages. However, detailed examination and precise interpretation of its drainage basin morphometries and their networks across different parts of the Handun anticline have not been considered. The Handun anticline displays a high variability in the morphometry of its drainage basins and their networks, and we use this variability to explore in detail and more precisely their relationships to tectonic activity.

Accordingly, the objectives of this study are to: (1) investigate the relationship between drainage basin orientation and the morphometric properties of the drainage basins and their networks; (2) to assess the variations of the analyzed morphometric parameters in three tectonic zones and the northern and southern limb flanks of the growing fold structure; and (3) evaluate the effects of lateral and vertical growth of the fold and its resulting fault trends on the drainage basin orientation.

Study area

Geological setting

The Zagros Fold and Thrust Belt (ZFTB), in which the study area is located, is one of the youngest continental collision belts in the world, extending over 1500 km from Kurdistan in northern Iraq to the Hormuz Strait at the mouth of the Persian Gulf. Folding in the Zagros Simply Folded Belt started in the early Miocene (Sherkati et al., 2005), and folds associated with the Zagros Foredeep are still growing (Berberian, 1995).

The Handun anticline is part of Bandar Abass region in the eastern termination of the ZFTB.

The Bandar Abbas region, also known as the hinterland, syntaxis, and embayment is a transitional area between three geological zones comprising 1) the Zagros collisional belt to the NW, 2) the Makran accretionary prism to the east, and 3) the Oman Mountains to the SE (Molinaro et al., 2004; Faridi et al., 2021). Two main characteristics of the eastern Zagros are: (1) numerous emergent or still buried salt diapirs, distributed irregularly across a wide region from the suture zone in the north to the Persian Gulf in the south; and (2) particular aspect ratios of folds, which are typically short and (compact) folds with irregular along strike shapes that frequently display a plan view ‘zigzag’ shape on maps and satellite imagery with marked changes in fold axis configuration (Jahani et al., 2009).

123 The Handun anticline in the Zagros Simply Folded Belt (ZSFB), located to the northeast of the
124 town of Fin in the Hormozgan province (Fig. 1) is the focus of this study. The anticline is
125 oriented E-W, with a length of 37 km, width of 9 km and area of 244.5 km^2. The anticline spans
126 an altitudinal range from 1840 m to 280 m. The Middle Miocene to Pleistocene syn-orogenic
127 coarsening upward sediments of the Agha Jari and Bakhtiyari Formations developed in central
128 parts of the Handun anticline show the minimum age of anticline is Pleistocene (Faridi et al.,
129 2021).

130 Lithological units of the anticline span the Pre-Cambrian, Cenozoic and the Quaternary (Fig.
131 2). The areas of Guri, Razak, Asmari-Jahrom, Hormuz, Quaternary, and Bakhtyari formations
132 are respectively 80%, 7.2%, 6.4%, 4.7%, 1.6%, and 0.1% of the whole study area. Two sets of
133 faults crosscut the Handun anticline, including (1) E-W trending faults, parallel to the fold axis;
134 and (2) NW-SE trending faults, oblique to the fold axis (Fig. 2). The Handun anticline occurs
135 within a zone of relatively high seismic activity (Berberian and Tchalenko, 1976). Some
136 historical and twentieth-century earthquakes have been recorded in the Bandar Abbas region
137 (Berberian et al., 1977; Berberian and Tchalenko, 1976; Ambraseys and Melville, 1982;
138 Berberian, 2014; Zare et al., 2014). Notable events include the Khurgu earthquake (21 March
139 1977 Mw 7), as one of the most destructive earthquakes in the Bandar Abbas region, occurring
140 ~ 15 km southeast of the Handun anticline.
141 Folds in the western branch of the syntaxis, in which the Handun anticline is located, have
142 higher aspect ratios (half wavelength/axial length), compared to the eastern branch of the
143 syntax which comprises long and thin folds with lower aspect ratios (Molinaro et al., 2004).
144 The Handun anticline is a faulted detachment fold (Molinaro et al., 2005, Ginés et al., 2019;
145 Faridi et al., 2021) with a salt core. In the Southeastern Zagros Folded belt, the Hormuz Series,
146 composed predominantly of the Late Precambrian Hormuz Salt formation (1–1.5 km-thick),
147 forms a basal viscous decollement influencing the wavelength, amplitude and style of folding

(Colman-Sadd, 1978; Sepehr and Cosgrove, 2004). According to Molinaro et al. (2004, 2005), folding developed first through the development of large detachment anticlines, followed by steep limbs of the most developed folds in the Southeastern Zagros that have already reached a more mature stage involving faulting within the forelimbs of the folds.

The Handun anticline comprises a salt diapir located at the fold culmination, exhibits a particular 'peanut-like' shape in plan view (Jahani et al., 2009). According to Jahani et al. (2009) the Handun diapir is now inactive with a wide empty crater, but shows growth strata in the Eocene-Oligocene levels and recycled Hormuz materials in Miocene beds, implying that the plug was near the surface before the Zagros orogeny and then emerged during folding. Due to the relative weakness of the salt and the strength of the surrounding wall-forming rocks, a strain gradient develops so that the central portion of the wall is squeezed more than the ends. With further fold shortening, a vertical weld develops, linking two remnant diapirs that have not been squeezed as much (Rowan and Vendeville, 2006). The core of Handun anticline is broken through by a salt diapir whose emergent top surface is now eroded away. According to the classification of salt diapirs of Eastern Fars based on their present-day surface morphology (Jahani et al., 2007), the Handun salt diapir is 'dead', comprising a highly eroded dome located within a near empty crater (type E: *sensu* Janhani et al., 2007).

Based on the Bandar Abbas synoptic station located approximately 50 km southeast of the study area, the mean annual precipitation, temperature and relative humidity (during 1980-2021 period) are 169.2 mm, 26.9 °C and 64.6%, respectively.

Geomorphic features

Based on the dip, topographic slopes, and width of limbs, the Handun anticline can be divided into 3 tectonic zones: western (W), central and eastern (E). The W and E zones encompass the

plunges of the anticline, whereas the central zone comprises the main anticlinal ridge and its limbs which are extensively eroded. In the western and eastern zones, the flanks of the plunging anticlinal limbs are incised by numerous low order consequent drainages and, in some cases, their orientation is changed by the fracture trends. As described by Ramsey et al. (2008), two wind gaps (abandoned / isolated dry valleys) are developed in the western plunge of the fold. The larger wind gap occurs as a ~ 5-km-long and 200-m-deep dry valley across the fold crest with several meanders. The second wind gap in the west comprises a shorter and straighter valley, cutting the tip of the fold. A 3rd wind gap can also be identified around the western nose of the anticline, where a deflected river around the fold nose has left a shallow wind gap (Fig. 3). Topographic cross-sections along the crest (AA′ profile), across the width of the fold (BB′, CC′, DD′, and EE′ profiles), and parallel to the hinge in the northern and southern limbs (FF′ and GG′) are shown in Fig. 4. The crest profile shows significant erosion of the central fold region, resulting in the formation of larger and more circular basins, especially on the southern limb. Transverse profiles across the fold demonstrate that the southern limb is more eroded compared to the northern one (BB′, and DD′ profiles). The plunged zones (BB′ and EE′ profiles) have gentler topographic gradients. However, these two display differences, where the eastern plunge (EE′) is more eroded compared to the western one (BB′). Profiles parallel to thehinge in the northern and southern limbs (FF′ and GG′) show higher erosion and entrenchment of the southern limb compared to the northern one. Evaluation of the fold crest line (Fig. 6) shows that the central part of the anticline is extensively eroded compared to the plunged zones, indicated by higher sinuosity along the anticline divide in the center, and lower values in the western and eastern zones (Table 1).

The combined effect of uplift and erosion of anticline has resulted in the formation of triangular facets along the southern limb of the central zone (Fig. 5). Erosion of these triangular facets acting concurrently with uplift of the mountain fronts has created V-shaped valleys, with their

197 wide upper parts and narrow outlets, known as ‘wine-glass’ forms on the steep slopes of
198 southern limb in the central portion of the anticline (Fig. 5a). Surface features of karst,
199 especially karren, are common geomorphic features on carbonate rocks of the Guri Member
200 (Fig. 5b).

201

202 **Materials and methods**

203 Faults, stratigraphic units, their lithologies and their collective spatial distributions were
204 derived from 1:100,000-scale geological maps (Gharabeili, 2005; Talebi, 2007). 57 drainage
205 basins developed into the anticline limbs were delineated based on Google Earth^{TM} images and
206 12.5 m resolution ALOS DEM data. Note that the 57 drainage basins are the main rivers whose
207 trunk streams originate at the main drainage divide of the anticline. Drainage networks were
208 digitized manually using Google Earth^{TM} images in combination with the 12.5 m ALOS DEM.
209 The mapped drainages were ordered according to Strahler system (Strahler, 1957) (Fig. 6).

210 Generally, the water flow direction is perpendicular to the contour lines, and hence the main
211 drainage networks flow perpendicular to the fold axis ((Jackson et al., 1998; Ramsey et al.,
212 2008). The main drainage network of a basin, formed on a fold flank, is oriented at a high angle
213 to the mountain front (close to 90^{o}), whereas it is oriented oblique to the mountain front line,
214 or fold axis, when it is affected by a fault trace or lateral growth of a fold (Ramsey et al., 2007;
215 Ramsey et al., 2008; Ribolini and Spagnolo, 2008; Castelltort et al., 2012; Krystopowicz et al.,
216 2020)

217 Thus, the degree of oblique orientation of the drainages with respect to the mountain front
218 can be diagnostic of active tectonic controls. In this study, a new geomorphic index, namely
219 the drainage basin orientation (DBO), is presented to evaluate the effect of active tectonics in

220 controlling the orientation of drainage developed into the flanks of an anticline. The DBO is
221 defined as:

222 $$DBO = |90 - \alpha|$$

223 where α is the angle between the mountain front line and the straight-line between the
224 endpoints of basin's main drainage (Fig. 7a). High values of DBO (i.e., larger than 15^{o}) reflect
225 basins affected by active tectonics such as faulting and lateral growth of folds. Very low DBO
226 values (close to 0) typically demonstrate 'normal' drainage basins little affected by active
227 tectonics. However, in some rare cases, drainage basins with lower DBO values (close to 0)
228 can be affected by faults trending perpendicular to the fold axis.

229 As a fold grows, all of the morphometric properties of drainage basins and their networks are
230 affected by active tectonics. In addition to the DBO index, other morphometric indices related
231 to drainage basins and their networks are used in this study: area (Ba), slope (S), asymmetry
232 factor (AF), hypsometric integral (HI), basin shape (Bs), crescentness index (CI), sinuosity of
233 main drainage (Smd), drainage density (Dd), drainage density of 1st-order streams (Dd1),
234 drainage frequency (Df), and sinuosity of anticline divides (Sad). The area and slope of
235 drainage basins were calculated using Integrated Land and Water Information System (ILWIS
236 3.3) software (ITC, 2007). The mean topographic slope (%) of each basin (S) was derived by
237 weighted average of all pixels of the slope map. The basin mid-lines were obtained using the
238 'Distance Calculation' function in the ILWIS software. The asymmetry factor (AF) is used to
239 calculate possible tectonic tilting of a drainage basin (Hare and Gardner, 1985; Keller and
240 Pinter, 2002; El Hamdouni et al., 2008). It is defined as: AF = 100(Ar/At), where Ar is the
241 drainage area on the right hand (facing downstream) of the main stream and At is the total area
242 of the drainage basin. In this study, the AF is expressed as the absolute value minus 50 (Peréz-
243 Peña et al., 2010):

244 $$AF = \left| 50 - \frac{Ar \times 100}{At} \right|$$

245 The basin shape (Bs) index is expressed as: Bl/Bw

246 where Bl is the length of basin mid-line and Bw is the width of the basin measured at its widest
247 point (see details in Bahrami et al., 2020). Drainage basins in tectonically active areas are
248 generally considered youthful and actively eroding and thus possess an elongated shape (higher
249 Bs value) (Ramírez-Herrera, 1998).
250 Drainage density (Dd) is defined as total stream length per unit area (Horton, 1932; Langbein,
251 1947). Drainage frequency is the total number of stream segments of all orders per unit area
252 (Devi et al., 2011). The first-order drainages are sensitive to tectonics and are important
253 indicators of areas with high rates of uplift (Zuchiewicz, 1998; Keller and Pinter, 2002). The
254 N1/N index, the ratio of 1st-order streams to the total number of streams of all orders, is
255 expected to increase in younger segments (plunges) of a laterally growing anticline. Drainage
256 density, drainage frequency, and the N1/N indexes can provide insights into the impact of
257 active tectonics on drainage networks (Devi et al., 2011; Melosh and Keller, 2013, Bahrami,
258 2022). In the older segments of tectonically active folds, drainage density and frequency are
259 more developed and have had more time to integrate or cannibalize other nearby drainages,
260 whereas the number of low-order streams are higher in the younger segments (noses) (Keller
261 and Pinter, 2002, Bahrami et al., 2020).

262

263 Sinuosity of main drainage (Smd) of a basin is expressed as:
264 Smd= Mc/SL
265 where Mc is the length of the main channel and SL is the length of the straight-line between
266 the endpoints of the main channel (Fig. 7b). The rate of uplift and slope gradient can affect the

values of channel sinuosity (Adams, 1980; Zámolyi et al., 2010; Joshi et al., 2013). It is expected that channel sinuosity is higher in the older and more uplifted segment of the anticline due to the higher lateral erosion of basins, whereas it is lower in the younger segments (noses) due to the presence of younger basins with lower erosion.

The hypsometric integral (HI) is calculated using an elevation-relief ratio (Strahler, 1952; Delcaillau et al., 1998; Bishop et al., 2002; Pavano et al., 2018). In this study, the 2nd order polynomial equation was fitted to the hypsometric curve, and then the fitted equation was integrated within the desired limits (0 to 1) to estimate the HI (Harlin, 1978; Singh et al., 2008; Liffner et al., 2018; Bahrami et al., 2020). High HI values typically reflect pronounced 'youthful' topography, likely corresponding to recent tectonic deformation. Low HI values are often related to 'older' landscape topography that has been exposed and thus eroded for a longer time period (Keller and Pinter, 2002; He et al., 2019).

The crescentness index (CI) (Bahrami et al., 2020) is defined as:

$$CI=LBM/SL$$

where LBM is the length of the basin mid-line and SL is the length of the straight-line between the endpoints of basin mid-line (Fig. 7c. High CI values (close to 1.5) are associated with entirely crescent-shaped basins, whereas the low CI values (close to 1) are straight basins (least crescent-shaped). The higher CI values relate to drainage basins developed on fold limbs, and these are considered as evidence for lateral fold growth (Bahrami et al., 2020).

Sinuosity of anticline divides (Sad) is a quantitative index related to fold morphometry. In the early stages of fold formation, the main drainage divide usually coincides with the fold hinge. As the fold grows over time, headward erosion of the basins formed on the fold limb flanks

290 will increase the sinuosity of the fold main drainage divide, hence forcing divergence between
291 the hinge and the main topographic divide. The ‘Sad’ is defined as (Bahrami et al., 2020):

292 Sad = LD/LH

293 where LD is the length of main divide of the anticline and LH is the hinge length (Fig. 7d).
294 Generally, higher Sad values are associated with the older, more eroded segment of the
295 anticline (core), whereas lower values are related to younger segments (noses) with lower
296 erosion.

297 To analyze correlations between variables, the Pearson's correlation coefficient (r) and
298 probability at 0.01 and 0.05 levels for the utilized morphometric parameters were calculated.
299 In order to compare the means of variables in two groups of basins (Northern limb/Southern
300 limb basins), the independent sample t-tests were calculated for different parameters. Tukey's
301 post -hoc test was performed to show statistically significant differences between pairs of
302 means (Zone1 versus zone 2, zone 1 versus zone 3, and zone 2 versus zone 3) for different
303 parameters.

304 The rock strength also plays a role in the morphometry of landforms and drainage networks
305 (Stokes and Mather, 2015). Although most of the study area (80%) is composed of the same
306 lithology (Guri Member), the exposure of some lithological units having various strengths in
307 the study area could exert some effect upon the morphometry of the basins and their drainage
308 networks. According to some studies focused on the relative strength of geological formations
309 in Iran (Sepehr and Honarmandnejad, 2012; Peyrowan and Shariatjafari, 2013), we categorized
310 the lithological formations of the study area into two strength types:

311 Type 1 (strong): Guri, Asmari–Jahrom, Bakhtiari,

312 Type 2 (weak): Hormuz Series, Razak, and Quaternary alluvial terraces and deposits

313 Basins that comprised >70% of type 1 were considered to have a 'strong' rock strength, 50 to
314 70% type 1 as 'intermediate' strength, and <50% type 1 as 'weak' strength.

315 **Results**

316 **Rates and variations of parameters**

317 The study area anticline and its 57 drainage basins across the three tectonic zones are shown in
318 Fig. 8. The morphometric properties of the studied drainage basins are summarized in Table 5.
319 Values of basin area range from 0.058 km^2 (basin 40 in the eastern zone) to 25.74 km^2 (basin
320 45 in the central zone). Amongst all basins, basin 1 (western zone) has the lowest topographic
321 slope (8.5%), whereas basin 34 (central zone) has the highest value (69.27%). Basin 7 (western
322 zone) is the most elongated (Bs= 11.43), whereas basin 31 (central zone) is the most circular
323 (Bs=1.165). The lowest HI value (0.41) is associated with basin 40 (eastern zone) whereas the
324 highest HI value (0.77) is related to basin 17 (western zone). The lowest value of asymmetry
325 factor (0.81 %) is related to basin 31 (central zone), and the highest value (35.2%) is associated
326 with basin 22 (western zone). Basin 1 (western zone) has lowest value of the crescentness index
327 (CI= 1.003) whereas basin 35 (central zone) is the most crescent-shaped (CI=1.344). The
328 lowest value of sinuosity of the main drainage (1.028) is associated with basin 56 (in the
329 western zone) whereas the highest value (2.57) is related to basin 52 (western zone). Values of
330 drainage basin orientation across the study area ranges from 0 (basin 30 in the central zone) to
331 46^o (basin 45 in the central zone).

332 **Tectonic zone results**

333 The values of the morphometric parameters of the drainage networks (Dd, Dd1, and Df), the
334 mean values of drainage basin properties (Ba, S, Bs, HI, AF, CI, Smd, and DBO), and the
335 sinuosity of the anticline drainage divide (Sad) across the 3 tectonic zones are given in Table
336 1. Results show that basins have a larger mean area in the central zone (4.02 km^2), compared

337 to the western and eastern zones (respectively 1.93 and 1.73 km^2). The mean of topographic
338 slope of basins in the central zone (54.81%) is higher compared to the western and eastern
339 zones (23.25% and 31.3% respectively). The central zone has relatively circular basins
340 compared to more elongated basins in the western and eastern zones. This is confirmed by the
341 lower mean value of Bs in the central zone (2.46) compared to higher mean Bs in the western
342 and eastern zones (5.34 and 4.58 respectively). Higher mean HI values in the western zone
343 (0.63), compared to those of the central and eastern zones (0.53 and 0.46 respectively) shows
344 that basins of the western zone have younger topography than other zones. Basins have higher
345 mean values of AF in the western zone (15.31), compared to the central and eastern zones
346 (12.48 and 5.53 respectively). Although the absolute value of AF increases from the western
347 zone towards the eastern zone, a regular trend in the direction of basin tilting is lacking. About
348 60% of basins in the western zone are tilted towards the west, whilst 50% of basins in the
349 central zone are tilted towards the west, and 67% of basins in the eastern zone are tilted towards
350 the north. The mean crescentness index (CI) is higher the central zone (1.13), compared to the
351 western and eastern zones (1.09 and 1.04 respectively). The mean sinuosity of main drainage
352 (Smd) of basins is higher in the central zone (1.24) than the western and eastern zones (1.19
353 and 1.16 respectively). The mean drainage basin orientation (DBO) is also higher in the central
354 zone (24.36o), compared to the western and eastern zones (22 o and 13.67 o respectively).
355 Results of the sinuosity of the anticline divide (Sad) show that the central zone of the anticline
356 is characterized by higher Sad values (1.37) compared to the northwestern and southeastern
357 noses (1.23 and 1.03 respectively).

358 As Fig. 9 shows, the median values of Ba, S, CI, and DBO are greater in the central zone
359 compared to western and eastern zones. In contrast, the median value of Bs is lower in the
360 central zone compared to the plunges. The median values of AF and HI decrease from western
361 zone towards eastern zone. The median values of Smd are fairly similar among three zones.

The ANOVA test results (Table 2) show that means of basin slope, basin shape, hypsometric integral, and asymmetry factor have statistically significant differences between three zones. Results of Tukey's post -hoc test show that zones 1 and 2 have statistically different means of basin slope, basin shape, and hypsometric integral. Zones 2 and 3 have statistically different means of basin slope. Zones 1 and 3 have statistically different means of hypsometrical integral. Overall, the means of most parameters including Ba, Bs, CI, Smd, DBO are fairly similar in zones 1 and 3 (plunges).

Limb results

Table 3 shows the morphometric parameters associated with drainage networks and the mean values of the morphometric indices related to the drainage basins for the southern and northern limbs of the anticline. The northern limb is characterized by steeper slopes, depicting more elongated and younger basins (higher S, Bs and HI values) with higher values of drainage basin orientation, compared to the southern limb. The values of drainage density, drainage frequency, and 1st order drainage density are also higher in the northern limb. The southern limb is characterized by larger basins, with higher values of asymmetry factor, crescentness index and sinuosity of main channel.

Box plots of the morphometric parameters in the northern and southern limbs of the Handun anticline are given in Fig. 10. The median values of Ba, AF, CI, and Smd are higher in the southern limb than northern one. The median values of S, Bs, Hi, and DBO are higher in the northern limb compared to the southern one. According to the t-test values (Table 4), there is statistically significant difference between mean of basin area in the northern and southern limbs.

Regression analysis

To evaluate the quality of the relationship between the resulting morphometric parameters, linear regressions were performed. Pearson's correlation coefficient (r) and confidence levels of $p = 0.01$ and $p = 0.05$ for different parameters are given in Table 6. Drainage basin orientation is strongly correlated with crescentness index, sinuosity of main channel, and basin area; so that the values of CI, Smd, and Ba increase with DBO. Basin area (Ba) is strongly positively correlated with the S, AF, CI, Smd, and DBO indexes, whereas it is strongly negatively correlated with Bs and HI (Table 6). Topographic slope (S) of basins has a strong positive correlation with CI, and a strong negative correlation with Bs. Basin shape (Bs) is strongly negatively correlated with CI and Smd. The crescentnes index (CI) of basins is strongly positively correlated with Smd and DBO.

Discussion

The Bandar Abbas syntaxis, as a transitional zone between the Zagros belt, the Makran convergence zone, and the Oman Mountains, hosts numerous salt diapirs. Lateral and vertical fold growth as well as the geodynamic history of a salt diapir in the central part of Handun anticline is likely to have strongly controlled the fold shape and the fluvial landscape morphometric properties. Geomorphic evidence, including a decrease in the fold limb dip towards the west and east (Fig. 2), a decrease in relief of the topographic profile along the fold crest towards the west and east (Fig.4), a decrease in the sinuosity of the anticline drainage divide (Sad) from the core of the anticline towards west and east (Table 1), development of fan-shaped and asymmetric forked drainage patterns in the western and eastern fold plunge regions (Fig. 6), and formation of three wind gaps around the western plunge of the anticline (Fig. 3) collectively demonstrate lateral propagation of the Handun anticline towards the west and east. In accordance with criteria of Hetzel (Hetzel et al., 2004; Keller and DeVecchio, 2022), a decrease in wind gap elevation towards west (Fig. 3) implies lateral growth of the Handun anticline towards the west. The decrease in elevations of the bases of the wind gaps

411 from east to west (Fig. 3), and the presence of a water gap flowing around the western nose of
412 the fold collectively reinforce the westwards lateral propagation of the Handun anticline. As
413 Fig. 5 shows, field geomorphological evidence demonstrates that wind gap 3 has been recently
414 abandoned. Development of the fan-shaped and asymmetric forked drainage network on the
415 fold plunges, especially that of the western one, is further strong evidence for lateral anticline
416 growth (Fig. 6). Most of the asymmetric forked drainage networks are observed in the southern
417 limb of the western zone, where the tributary headwaters (often 1st order drainages) have been
418 curved towards the central parts of the anticline. The development of triangular facets and
419 wine-glass valleys in the central zone (Fig. 5), and the lack of these features in the western and
420 eastern zones, depicts a youthful topography with less erosion, also implying lateral fold
421 growth.

422 Results show that the older and high-amplitude segment of the fold (central zone) is
423 characterized by larger and relatively circular basins, and a higher sinuosity of its anticlinal
424 ridge drainage divide (Sad), implying dominance of lateral and headward erosion. In contrast,
425 the smaller and highly elongated basins in the plunge areas (western and eastern zone) depict
426 less eroded and younger topography. Data shows that the western and eastern plunges have
427 lower values of topographic slope, indicating a more youthful topography due to the less
428 marked amplitudes of these zones, compared with central zone with its high-amplitude and
429 steep-sloped topography. It is expected that values of the hypsometric integral would be lower
430 in the central zone of anticline compared to the plunges. Results show that the mean HI is
431 higher in the western zone than that of the central zone, whereas the mean HI is lower in the
432 eastern zone than that of the central zone (Table 1). This confirms a more youthful topography
433 for the western fold plunge and active lateral growth towards the west. The absolute values of
434 the asymmetry factor increase from the eastern zone towards the western zone. It is expected
435 that basins formed in the western and eastern zones will be tilted towards the fold tips, because

436 the topographic slopes and the dip of the strata are generally towards the fold noses.
437 Nevertheless, a regular trend in the direction of basin tilting is lacking (Fig. 8). Bahrami et al.
438 (2020) attributed this lack of regular trend in the direction of basin tilting in the Gorm anticline
439 (Fars region), to the curvature or crescentness of the drainage basins and their main channels.
440 They argued that in the initial stages of the fold growth, the main drainage of elongated basins
441 migrates towards the fold tip. With increasing lateral growth of the fold, the headwater areas
442 of the basins tend to be curved towards the center of the fold and, hence, a crescent-shaped
443 basin can form. In this stage, the upstream segment of the main channel migrates perpendicular
444 to the hinge, towards adjacent syncline, and hence tends to decrease the drainage area on the
445 right hand (facing downstream) of the trunk stream. Therefore, the upstream and downstream
446 segments of the main drainage of a crescent-shaped basin affect the asymmetry factor in a
447 reverse manner, so that the downstream part of the trunk channel tends to increase the drainage
448 area on the right hand of the trunk stream, whereas the upstream part of main channel tends to
449 decrease it (see Fig. 14 in Bahrami et al., 2020).

450 Results show that the southern limb is characterized by larger basins, with higher values of
451 asymmetry factor, crescentness index and sinuosity of the main channels (Table 3), suggesting
452 a higher lateral erosion of this limb. In contrast, steeper slopes, highly elongated and younger
453 basins (higher, Bs, Bs, and HI values) with higher values of drainage basin orientation in the
454 northern limb reflect a more youthful topography and lower erosion.

455 Note that values of the crescentness index and sinuosity of the main channels are higher in the
456 central zone compared to the western and eastern fold plunge zones (Table 1). Generally, in
457 the older and more uplifted segment of the central zone, the main drainages of the basins are
458 more sinuous due to the lateral erosion of these basins. Also, due to this lateral erosion, basins
459 are more crescent-shaped in the central zone, whereas younger basins of the western and
460 eastern zones with lower erosion have lower values of CI and Smd.

Although different geomorphological evidence of lateral and vertical growth of folds have been proposed (Keller et al., 1999; Azor et al., 2002; Ramsey et al., 2008; Bretis et al., 2011; Bahrami, 2013; Collignon et al., 2016; Bahrami et al., 2020), all of the geomorphic evidence associated with fold growth may not be evident from a given fold because of erosion. Hence, new geomorphic indicators are required to detect lateral fold growth. In this study, a new morphometric index, drainage basin orientation (DBO), was calculated for 57 basins in three tectonic zones of anticline and its relation with other morphometric parameters were evaluated. Results show that drainage basin orientation is strongly correlated with crescentness index, basin area, and sinuosity of main drainage, implying that the value of drainage basin orientation is higher in larger and more crescent-shaped basins with more sinuous main drainage (Table 6). The mean values of DBO, Ba, CI, are higher in the central zone, compared to the western and eastern zones, suggesting that more eroded central zone is marked by the larger and more crescent-shaped basins with more sinuous main drainages. Although the mean value of drainage basin orientation is higher in the central zone, the mean DBO is also high in the western and eastern plunges. Overall, the high values of DBO in the Handun anticline can be explained as follows:

(1) The main reason for increased drainage basin orientation in the fold plunge zones (western and eastern zones) is the presence of an asymmetric forked drainage pattern or curved drainages. In the early stages of fold growth, drainages are either not curved or are less curved, whereas with progressive lateral growth of the fold over time, headwater tributaries become curved towards the core of the anticline, and hence a crescent-shaped basin can develop on the fold plunges (Fig. 11). The general trends of the main channel of these crescent-shaped basins that are often oblique to the fold axis, have resulted in the increased values of drainage basin orientation (DBO) in the western and eastern zones. This situation is in accordance with the finding of Bahrami et al.

(2020) study, demonstrated the development of crescent-shaped basins in the pre-nose segment of Gorm anticline in Fars area, where the upstream parts of basins have been curved towards the central part of the anticline.

(2) Faults and fractures can also affect the trends of the DBO. Major faults of the Zagros Simply Folded Belt include belt-parallel faults and belt-oblique faults (Sepehr and Cosgrove, 2007). Aside from major faults, there are numerous fractures with different trends formed on the folds. Although precise information about the kinematics between the folds and faults are not available for the study area anticline, the findings of some studies from different parts of the Zagros have shown that minor faults and fracture systems are related to either folds, or major basement faults (such as Sarvestan, Bala Rud, Kazerun, Izeh, and Anaran faults) with strike-slip deformation (Mobasher and Babaie, 2008; Tavani et al., 2014; Joudaki et al., 2016). The fold-related fractures are the axial (FA), cross-axial (FC), and two oblique (FO1 and FO2) fracture sets (Mobasher and Babaie, 2008; Joudaki et al., 2016). Fractures associated with major basement faults are five sets (including: synthetic Riedel shear fractures (R); antithetic Riedel shear fractures (R ′); synthetic P-shear fractures; Y-shear fractures, parallel to the main strike-slip fault; and extensional T-set fractures, parallel to the principal shortening direction (Z) (Mobasher and Babaie). Among these fractures, oblique fractures as well as extensional fractures oriented parallel to the anticline axes have exerted a major control in the increase of drainage basin orientation. For example, the main drainages of basins 10, 16, 18, and 19, with high DBO values (Table 5) coincide with oblique fractures in the western zone (Fig. 12). Also, with progressive growth of the anticline over time, oblique faults or fractures can join to the normal faults or fractures oriented parallel to the fold axis (Fig. 13), and thereby curved drainages with high DBO values are formed. Overall, Numerous faults and fractures oriented oblique

511 and parallel to the fold axis in some anticlines of Zagros belt such as Anaran (Joudaki
512 et al., 2016), Kuhe-Asmari (McQuillan, 1973; Carminati et al., 2013), Bankol
513 (Bahrami, 2022), Sim (Carminati et al., 2013), Kabir-Kuh (Pireh et al., 2006),
514 Bangestan (Tavani et al., 2011), Dil, Khami, and Sulak (Ahmadhadi et al., 2008)
515 anticlines have developed. These faults and major fractures play an important role in
516 the orientation of drainages and their basins on the limbs of folds.
517 (3) The salt diapir located in the core of the fold also controls the drainage configuration
518 and hence drainage basin orientation in the central zone. In maturely eroded domes such
519 as the study area one, where curved outcrops of alternating resistant/weak sedimentary
520 layers are developed around the salt diapir, a ridge (in resistant rocks) and valley (in
521 soft layers) topography is formed. In this semi-annular drainage pattern, the main
522 drainages are arranged into a circular pattern with subsidiary drainages configured at
523 right angles to them. As Fig. 14 shows, this drainage pattern in the southern part of salt
524 diapir in the central zone has developed some curved main drainages resulting in the
525 increase of the values of drainage basin orientation (i.e., basins 45 with high DBO
526 value).
527 (4) The tectonic geomorphic history of the basins also controls the value of drainage basin
528 orientation. Although the value of DBO is increasing from noses towards the fold
529 central part, some basins (52 and 55) around the fold nose have higher values of DBO
530 and CI. The positions of basins 52 and 55 coincide with wind gaps 1 and 2 in the western
531 plunge (Figs. 3 and 8), where the abandonment of river channels has resulted in the
532 formation of dry valleys that are now crescent-shaped basins in which their main
533 channels are oriented oblique to the fold axis. Specifically, basin 52 (coincides with
534 wind gap 1) with high value of drainage basin orientation (43^{o}), and crescentness index
535 (1.31), and highest value of sinuosity of main channel (2.57) amongst all basins,

comprises an abandoned deeply entrenched, meandering channel. This shows that tectonic geomorphic history of basins can exert an important role in the present day orientation and other morphometric properties of channels and basins.

Comparison of the morphometric properties of drainage networks across the three tectonic zones shows that values of drainage density (Dd), 1st order drainage density (Dd1), and drainage frequency (Df) are higher in the plunges (western and eastern zone) compared to the central zone (Table 1). Higher values of the1st order drainage density in the plunges especially the western plunge shows younger and less-developed drainage networks in these areas. Results also shows that values of Dd, Dd1 and Df are higher in the less-eroded and steeply-sloped northern limb, compared with highly-eroded southern limb. Hence, results imply that more eroded parts of the anticline (central zone and southern limb) have lower drainage density and frequency, compared to the younger and less-eroded segments of the Handun anticline.

Fig. 14 shows the spatial variation in drainage pattern in different parts of the anticline. A fan-shaped drainage pattern is developed around the ends of the anticline noses. A dendritic drainage pattern is observed in the central zone. Parallel and curved parallel drainage patterns are developed in the western and eastern zones. Radial drainage pattern is observed in the central zone. An asymmetric forked drainage pattern is developed on the southern limb of the western zone, especially in the pre-nose area. A semi-annular drainage pattern is developed around the salt diapir in the core of anticline (Basin 44) (Fig. 14).

The effect of lithology should also be considered as a secondary factor in decreasing values of Hypsometric integral and basin shape. Results show that nearly all basins (except basins 37, 43 and 45) are dominated by strong bedrocks. Basins 37 and 45 in the central zone are characterized by weak strength rocks, as <50% of these basins are composed of rock type 1 (strong). Basin 43 in the eastern zone is characterized by intermediate strength rocks, as 50 to

70% of these basins are composed of rock type 1. Hence, the lithological effect should also be considered in decreasing values of HI and Bs indexes in the central and eastern zones, where the exposure of some soft rocks has facilitated the lateral and vertical erosion and hence decreasing HI and Bs indexes.

Conclusion

Drainage basins and their networks formed on an actively growing anticline are affected by the interaction of surface processes and active tectonics affecting the folds. The Handun anticline in the Bandar Abass region, as part of the hinterland or syntaxis, is a transitional area between three geological zones of the Zagros collisional belt to the NW, the Makran accretionary prism to the east, and the Oman Mountains to the SE. The salt-cored Handun anticline with numerous drainage basins, often oriented oblique to the fold axis, was selected to analyze the effect of active tectonics on the drainage basin orientation and other morphometric parameters of basins and their networks. Data show that drainage basin orientation is strongly correlated with crescentness index, basin area, and sinuosity of main drainage, implying that the value of drainage basin orientation is higher in larger and more crescent-shaped basins with more sinuous main drainage. The mean values of drainage basin orientation, basin area, crescentness index are higher in the central zone, compared to the western and eastern zones, suggesting that more eroded central zone is marked by the larger and more crescent-shaped basins with more sinuous main drainages. Southern flank of anticline is characterized by larger basins, with higher values of asymmetry factor, crescentness index and sinuosity of main channel, implying the higher lateral erosion, while steeper slopes, highly elongated and younger basins (higher, Bs, Bs, and HI values) with higher value of drainage basin orientation in the northern limb imply the youthful of topography and lower erosion.

583 It is worth noting that although the values of drainage basin orientation are higher in the central
584 zone, the mean DBO is also high in the western and eastern plunges. The high DBO value can
585 be attributed to four parameters: (1) the presence of asymmetric forked drainage pattern or
586 curved drainages, which their general trends are often oblique to the fold axis, resulted in the
587 increased values of drainage basin orientation in the western and eastern zones; (2) the trend
588 of faults and fractures, especially oblique fractures oriented parallel to the anticline axis that
589 exert strong control in the increase of drainage basin orientation; (3) the semi-annular drainage
590 pattern formed around the salt diapir located in the core of the fold, in which main drainages
591 are arranged in a circular pattern with subsidiary drainages lying at right angles to them,
592 resulting in the increased values of drainage basin orientation; and (4) tectonic geomorphic
593 history of basins, so that some basins (52 and 55), with higher values of DBO, coincide with
594 wind gaps 1 and 2 in the western plunge, where the abandonment of river channels has caused
595 the formation of dry valleys that are now crescent-shape basins in which their main channels
596 are oriented oblique to the fold axis.

597 Overall, a decrease in the values of sinuosity of anticline divide, drainage basin orientation,
598 and crescentness index from the core of anticline towards west and east, development of fan-
599 shaped and asymmetric forked drainage patterns in the western and eastern plunge, formation
600 of three wind gaps around the western plunge of the anticline, imply the lateral propagation of
601 Handun anticline towards west and east.

602 **Declaration of Competing Interest**

603 The author declare that he has no known competing financial interests or personal relationships
604 that could have appeared to influence the work reported in this paper.

605

606 **References**

607 Adams, J., 1980. Active tilting of the United States midcontinent: geodetic and geomorphic
608 evidence. Geology 8, 442-446.
609 Adeoti, B., Webb., A.A.G., 2022. Geomorphology of contractional salt tectonics along the
610 Kuqa fold-thrust belt, northwestern China: Testing pre-kinematic diapir versus source-
611 fed thrust and detachment fold models. Journal of Structural Geology 161, 104638.
612 Altin, T.b., Altin, B.N., 2011. Development and morphometry of drainage network in volcanic
613 terrain, CentralAnatolia, Turkey. Geomorphology 125, 485–503.
614 Ambraseys, N.N., Melville, C.P., 1982. A history of Persian Earthquakes, Cambridge Earth
615 Science Series, Cambridge University Press, London.
616 Azor, A., Keller, E.A., Yeats, R.S., 2002. Geomorphic indicators of active fold growth: South
617 Mountain–Oak Ridge anticline, Ventura basin, southern California. Geol. Soc. Am.
618 Bull. 114 (6), 745–753.
619 Bahrami, S., 2013. Analyzing the drainage system anomaly of Zagros basins: implications for
620 active tectonics. Tectonophysics 608, 914–928.
621 Bahrami, S., 2022. Analysis of confluence angle of drainages and its relation to morphometric
622 properties of drainage basins in the Zagros Simply Folded Belt, Iran. Geomorphology
623 400, 108091.
624 Bahrami, S., Capolongo, D., Rahdan Mofrad, M., 2020. Morphometry of drainage basins and
625 stream networks as an indicator of active fold growth (Gorm anticline, Fars Province,
626 Iran). Geomorphology 355, 107086.
627 Berberian, M., 1995. Master ‘blind’ thrust faults hidden under the Zagros folds: active
628 basement tectonics and surface morphotextonics. Tectonophysics 241, 193–224.
629 Berberian, M., 2014. Earthquakes and Coseismic Surface Faulting on the Iranian Plateau; A
630 Historical, Social, and Physical Approach (Developments in Earth Surface Processes
631 17). Elsevier, Amsterdam, Netherlands (776 pp.)
632 Berberian, M., Tchalenko, J.S., 1976. Earthquakes of Bandar Abbas-Hadji-Abad region,
633 Zagros (Iran). In: Berberian, M. (Ed.), Contribution to the Seismotectonics of Iran, Part
634 II. vol. 39. Geol. Surv. Iran, pp. 371–396.
635 Berberian, M., Papastamatiou, D., Qoraishi, M., 1977. Khurgu (north Bandar Abbas-Iran)
636 earthquake of March 21, 1977: a preliminary field report and a seismotectonic
637 discussion. In: Berberian, M. (Ed.), Contribution to the Seismotectonics of Iran, Part
638 III. Geol. Min. Surv. Iran, vol. 40, pp. 7–50.
639 Bishop, M., Shroder, J., Bonk, R., Olsenholler, J., 2002. Geomorphic Change in High
640 Mountains: A Western Himalayan Perspective. Global Planetary Change 32, 311-329.

641 Bretis, B., Bartl, N., Grasemann, B., 2011. Lateral fold growth and linkage in the Zagros fold
642 and thrust belt (Kurdistan, NE Iraq). Basin Res. 23, 615–630.
643 Castelltort, S., Goren, L., Willett, S.D., Champagnac, J.D., Herman, F., Braun, J., 2012. River
644 drainage patterns in the New Zealand Alps 384 primarily controlled by plate tectonic
645 strain. Nature Geoscience 5 (10), 744–8
646 Collignon, M., Fernandez, N., Kaus, B.J.P., 2015. Influence of surface processes and initial
647 topography on lateral fold growth and fold linkage mode. Tectonics 34. https://doi.
648 org/10.1002/2015TC003843.
649 Collignon, M., Yamato, P., Castelltort, S., Kaus, B.J.P., 2016. Modeling of wind gap formation
650 and development of sedimentary basins during fold growth: application to the Zagros
651 Fold Belt, Iran. Earth Surf. Process. Landf. 41, 1521–1535.
652 Colman-Sadd, S.P., 1978. Fold development in Zagros simply folded belt, southwest Iran. Am.
653 Assoc. Pet. Geol. Bull. 62, 984–1003.
654 Delcaillau, B., Carozza, J.M., Laville, E., 2006. Recent fold growth and drainage development:
655 the Janauri and Chandigarh anticlines in the Siwalik foothills, northwest India.
656 Geomorphology 76, 241–256.
657 Delcaillau, B., Deffontaines, B., Angelier, J., Déramond, J., Floissac, L., Souquet, P., Chu,
658 H.T., 1998. Morphotectonic evidence from lateral propagation of an activefrontal fold;
659 the Pakuashan anticline, foothills of Taiwan. Geomorphology 24, 263–290.
660 Devi, R.K.M., Bhakuni, S.S., Bora, P.K., 2011. Tectonic implication of drainage set-up in the
661 Sub-Himalaya: a case study of Papumpare district, Arunachal Himalaya, India.
662 Geomorphology 127, 14–31.
663 El Hamdouni, R., Irigaray, C., Fernndez, T., Chacon, J., Keller, E.A., 2008. Assessment of
664 relative active tectonics, southwest border of the Sierra Nevada (Southern Spain).
665 Geomorphology 96, 150–173.
666 Faghih, A., Nourbakhsh, A., 2014. Appraisal of relative tectonic activity along the Kazerun
667 Fault Zone, Zagros Mountains, Iran: insight from spatial analysis of geomorphic
668 indices. Geol. J. https://doi.org/10.1002/gj.2597.
669 Faridi, P., Rezaee, P., Piryaei, A., Masoodi, Masoodi, Masoodi, M., 2021. Halokinetic
670 sequences as indicators of Cenozoic diapiric growth: The Handun Salt Diapir (SE
671 Zagros, Bandar Abbas). Geopersia 11(2), 299-317.
672 García-Delgado, H., Velandia, F., 2020. Tectonic geomorphology of the Serranía de San Lucas
673 Central Cordillera): Regional implications for active tectonics and drainage
674 rearrangement in the Northern Andes. Geomorphology 349, 106914.

675 Gharabeili, G.R., 2005. 1:100000 Geologic Map of Fin (Sheet 20870E). National Iranian Oil
676 Company.
677 Ginés, J., Edwards, R., Lohr, T., Larkin, H. and Holley, R., 2019. Remote sensing applications
678 in the Fars Region of the Zagros Mountains of Iran. Geological Society, London,
679 Special Publications, 490, 417-444.
680 Hare, P.W., Gardner, T.W., 1985. Geomorphic indicators of vertical neotectonism along
681 converging plate margins, Nicoya Peninsula, Costa Rica. In: Morisawa, M., Hack, J.T.
682 (Eds.), Tectonic Geomorphology. Proceedings of the 15th Annual Binghamton
683 Geomorphology Symposium. Allen and Unwin, Boston, MA, pp. 123–134.
684 Harlin, J.M., 1978. Statistical moments of the hypsometric curve and its density function.
685 Journal of the International Association for Mathematical Geology, 10(1), 59–72
686 He, C., Rao, G., Yang, R., Hu, J., Yao, Q., Yang, C-J., 2019. Divide migration in response to
687 asymmetric uplift: Insights from the Wula Shan horst, North China. Geomorphology
688 339, 44–57.
689 Hetzel, R., Tao, M., Niedernann, S., Strecker, M., Ivy-Ochs, S., Kubik, P., Gao, B., 2004.
690 Implications of the fault scaling law for the growth of topography: Mountain ranges in
691 the broken foreland of north-East Tibet. Terra Nova 16 (3), 157–162.
692 Horton, R.E., 1932. Drainage basin characteristics. Trans. Am. Geophys. Union 13, 350–361.
693 ITC, 2007. Integrated Land and Water Information System (ILWIS). ITC, The Netherlands.
694 http://www.itc.nl/ ilwis33.asp.
695 Jahani, S., Callot, J.P., Frizon de Lamotte, D., Letouzey, J., Leturmy, P., 2007. The salt diapirs
696 of the eastern Fars province (Zagros, Iran): A brief outline of their past and present, in:
697 Thrust Belt and Foreland Basin, edited by O. Lacombe et al., pp. 289 – 308, Springer,
698 Berlin.
699 Jahani, S., Callot, J. P., Letouzey, J., Frizon de Lamotte, D., 2009. The eastern termination of
700 the Zagros Fold and Thrust Belt, Iran: Structures, evolution, and relationships between
701 salt plugs, folding, and faulting. Tectonics 28(6),
702 C6004. https://doi.org/10.1029/2008TC002418.
703 Jackson, J., Van Dissen, R., Berryman K., 1998. Tilting of active folds and faults in the
704 Manawatu region, New Zealand: evidence from surface drainage patterns. New
705 Zealand Journal of Geology and Geophysics 41, 377–385.
706 Joshi, P.N., Maurya, D.M., Chamyal, L.S., 2013. Morphotectonic segmentation and spatial
707 variability of neotectonic activity along the Narmada–Son Fault, Western India:
708 Remote sensing and GIS analysis. Geomorphology 180-181, 292-306.

709 Joudaki, M., Farzipour-Saein, A., Nilfouroushan, F., 2016. Kinematics and surface fracture
710 pattern of the Anaran basement fault zone in NW of the Zagros fold-thrust belt. Int. J.
711 Earth Sci. 105 (3), 869–883.
712 Keller, E.A., DeVecchio, D.E., 2022. Tectonic geomorphology of active folding and
713 development of transverse drainages. In: Treatise on Geomorphology (second edition).
714 Elsevier Inc., pp. 477–494.
715 Keller, E.A., Gurrola, L., Tierney, T.E., 1999. Geomorphic criteria to determine direction of
716 lateral propagation of reverse faulting and folding. Geology 27, 515–518.
717 Keller, E.A., Pinter, N., 2002. Active Tectonics: Earthquakes, Uplift, and Landscape (Second
718 Edition): Englewood Cliffs. Prentice Hall, New Jersey (362 pp.).
719 Krystopowicz, N.J., Schoenbohm, L.M., Rimando, J., Brocard, G., Rojay, B., 2020. Tectonic
720 geomorphology and Plio-Quaternary structural evolution of the Tuzgölü fault zone,
721 Turkey: Implications for deformation in the interior of the Central Anatolian Plateau.
722 Geosphere 16 (5), 1107–1124.
723 Langbein, W.B., 1947. Topographic characteristics of drainage basins. U.S. Geol. Surv., Water
724 Supply Pap., 968C, 125-157.
725 Lees, G.M., Falcon, N.L., 1952. The geographical history of the Mesopotamian Plains. The
726 Geographical Journal 118, 24–39.
727 Liffner, J.W., Hewa, G.A., Peel, M.C., 2018. The sensitivity of catchment hypsometry and
728 hypsometric properties to DEM resolution and polynomial order. Geomorphology 309,
729 112–120.
730 Machuca, S., García-Delgado, H., Velandia, F., 2021. Studying active fault-related folding on
731 tectonically inverted orogens: a case study at the Yariguíes Range in the Colombian
732 Northern Andes. Geomorphology 375, 107515.
733 Melosh, B.L., Keller, E.A., 2013. Effects of active folding and reverse faulting on stream
734 channel evolution, Santa Barbara Fold Belt, California. Geomorphology 186, 119–135.
735 Mobasher, K., Babaie, H.a., 2008. Kinematic significance of fold- and fault-related fracture
736 systems in the Zagros mountains, southern Iran. Tectonophysics 451, 156–169.
737 Molinaro, M., Guezou, J.C., P. Leturmy, P., Eshraghi, S.A., de Lamotte, D.F., 2004. The origin
738 of changes in structural style across the Bandar Abbas syntaxis, SE Zagros (Iran), Mar.
739 Pet. Geol. 21, 735 – 752.
740 Molinaro, M., Leturmy, P., Guezou, J. C., de Lamotte, D. F., Eshraghi, S. A., 2005. The
741 structure and kinematics of the southeastern Zagros fold thrust belt, Iran: From thin
742 skinned to thick skinned tectonics. Tectonics, 24(3), TC3007.

743 Özkaymak, Ç., Sözbilir, H., 2012., Tectonic geomorphology of the Spildağı High Ranges,
744 western Anatolia. Geomorphology 173–174, 128–140.
745 Pavano, F., Catalano, S., Romagnoli, G., Tortorici, G., 2018. Hypsometry and relief analysis
746 of the southern termination of the Calabrian arc, NE-Sicily (southern Italy).
747 Geomorphology 304, 74–88.
748 Peréz-Peña, J.V., Azor, A., Azañon, J.M., Keller, E.A., 2010. Active tectonics in the Sierra
749 Nevada (Betic Cordillera, SE Spain): insights from geomorphic indexes and drainage
750 pattern analysis. Geomorphology 119, 74–87.
751 Peyrowan, H.R., Shariatjafari, M., 2013. Presentation of a comprehensive method for
752 determining erodibility rate of rock units with a review on Iranian geology. J.
753 Watershed Eng. Manag. 5 (3), 199–213 (in Persian).
754 Ramírez-Herrera, M.T., 1998. Geomorphic assessment of active tectonics in the Acambay
755 Graben, Mexican volcanic belt. Earth Surf. Process. Landf. 23, 317–332.
756 Ramsey, L.A., Walker, R.T., Jackson, J., 2007. Geomorphic constraints on the active tectonics
757 of southern Taiwan. Geophys. J. Int. 170, 1357–1372.
758 Ramsey, L.A., Walker, R.T., Jackson, J., 2008. Fold evolution and drainage development in
759 the Zagros mountains of Fars province, SE Iran. Basin Res. 20, 23–48.
760 Ribolini, A., Spagnolo, M., 2008. Drainage network geometry versus tectonics in the Argentera
761 Massif (French–Italian Alps). Geomorphology 93, 253–266.
762 Rowan, M. G., Vendeville, B.C., 2006. Foldbelts with early salt withdrawal and diapirism:
763 Physical model and examples from the northern Gulf of Mexico and the Flinders
764 Ranges, Australia, Mar. Pet. Geol. 23 (9 – 10), 871 – 891.
765 Różycka, M., Migoń, P., 2021. Morphometric properties of river basins as indicators of relative
766 tectonic activity – Problems of data handling and interpretation. Geomorphology 389,
767 107807.
768 Sepehr, M., Cosgrove, J.W., 2004. Structural framework of the Zagros fold-thrust belt, Iran.
769 Mar. Pet. Geol. 21, 829–843.
770 Sepehr, M., Cosgrove, J.W., 2007. The role of major fault zones in controlling the geometry
771 and spatial organisation of structures in the Zagros Fold-Thrust Belt. In: Ries, A.C.,
772 Butler, R.W.H., Graham, R.H. (Eds.), Deformation of the Continental Crust: The
773 Legacy of Mike Coward. 272. Geological Society, London, Special Publications, pp.
774 419–436.

Sepehr, A., Honarmandnejad, S., 2012. Actual soil erosion risk mapping using modified CORINE method (case study: Jahrom Basin). Geogr. Environ. Hazards 3, 57–72 (in Persian).

Sherkati, S., Molinaro, M., Frizon de Lamotte, D., Letouzey, J., 2005. Detachment folding in the Central and Eastern Zagros fold-belt (Iran): salt mobility, multiple detachments and late basement control. J. Struct. Geol. 27 (9), 1680–1696.

Singh, O., Sarangi, A., Sharma, M.C., 2008. Hypsometric Integral Estimation Methods and its Relevance on Erosion Status of North-Western Lesser Himalayan Watersheds. Water Resources Management 22, 1545-1560.

Stokes, M., Mather, A.E., 2015. Controls on modern tributary-junction alluvial fan occurrence and morphology: high Atlas Mountains, Morocco. Geomorphology 248, 344–362.

Strahler, A.N., 1952. Hypsometric (Area-Altitude) Analysis of Erosional Topography. Geological Society of America Bulletin 63, 1117-1141.

Strahler, A.N., 1957. Quantitative analysis of watershed geomorphology. Trans. Am. Geophys. Union 38, 913–920.

Talebi, A., 2007. 1:100000 Geologic Map of Khoshangan (Sheet 20870E). National Iranian Oil Company.

Tavani, S., Snidero, M., Muñoz, J.A., 2014. Uplift-induced residual strain release and latethrusting extension in the Anaran mountain front anticline, Zagros (Iran). Tectonophysics 636, 257–269.

Wells, S.G., Bullard, T.F., Menges, C.M., Drake, P.G., Karas, P.A., Kelson, K.I., Ritter, J.B., Wesling, J.R., 1988. Regional variations in tectonic geomorphology along a segmented convergent plate boundary, Pacific coast of Costa Rica. Geomorphology 1, 239–265.

Woodbridge, K.P., Pirasteh, S., Parsons, D.R., 2019. Investigating fold-river interactions for major rivers using a scheme of remotely sensed characteristics of river and fold geomorphology. Remote Sens. 11, 2037. https://doi.org/10.3390/rs11172037.

Zámolyi, A., Székely, B., Draganits, E., Timár, G., 2010 Neotectonic control on river sinuosity at the western margin of the Little Hungarian Plain. Geomorphology 122, 231–243.

Zare, M., Amini, H., Yazdi, P., Sesetyan, K., Demircioglu, M.B., Kalafat, D., et al. 2014. Recent developments of the Middle East catalog. J. Seismol. 18(4):749-772.

Zuchiewicz, W., 1998. Quaternary tectonics of the Outer West Carpathians, Poland. Tectonophysics 297, 121–132.

807

808

809

Table captions

Table 1. Mean values of morphometric properties of 57 basins. Basins 1 to 25 and 46 to 57 are in the Western zone, basins 26 to 37 and 44 to 45 are in the central zone, and basins 38 to 43 are in the eastern zone. N is the number of basins.

Table 2. The P-values for ANOVA test (Between Zones), and Tukey's post–hoc test. Marked correlations (bold) are significant at the significance level of p = 0.05.

Table 3. Mean values of morphometric parameters associated with drainage networks (Dd, Dd1, and Df), sinuosity of anticline divide (Sad) and the means of the morphometric properties related to the drainage basins (Ba, S, Bs, HI, AF, CI, Smd, and DBO) in the northern and southern limbs of the anticline. N is the number of basins.

Table 4. The t-test results comparing means of variables in Northern limb/Southern limb basins. Marked correlations (bold) are significant at the significance level of p = 0.05.

Table 5. Summary of drainage basin and their network parameters.

Table 6. Pearson's correlation matrix for morphometric properties of studied basins.

Figure captions

Fig. 1. Regional study location map and detailed topography of the Handun anticline (red line) based on 12.5 m ALOS DEM data.

Fig. 2. Geological map of the Handun anticline and three geological cross-sections in the western nose (AB), central part (C-D), and eastern nose (E-F). Hs; Hormuz Series (salt, gypsum, shale, sandstone and limestone, and igneous rocks), As-Ja; Asmari-Jahrom (limestone and dolomitic limestone), Rz; Razak (marl, siltstone, sandstone and gypsum), Grm; Guri Member (limestone), Bk; Bakhtyari (conglomerate, sandstone, marl), Qt; Quaternary alluvial terraces and deposits.

Fig. 3. Topographic profile (A-B) showing the wind (W1, W2, and W3) and water gaps developed around the western end of the plunging anticline nose.

Fig. 4. Topographic profiles along the fold crest (AA′), across the width of the fold (BB′, CC′, DD′, and EE′), and parallel to the hinge in the northern and southern limbs (FF′ and GG′),

Fig. 5. Major landforms and processes of the Handun anticline; (a) triangular facets, composed of carbonate rocks of the Guri Member, developed in the steeply-sloped southern limb of the central zone; (b) small rillen-karren developed into carbonate rocks of the Guri Member; (c) dry valley (wind gap 1 [W1 in Fig. 3]) formed in the western plunge of the fold; (d) small dry

842 valley (wind gap 2 [W2 in Fig. 3]) developed in the western plunge of the fold; (e) recently
843 formed dry valley (wind gap 3 [W3 in Fig. 3]) developed around the western end of anticline
844 nose.

845 Fig. 6. Drainage map of the Handun anticline and its fold structure zonation.

846 Fig. 7. Graphical summary of methods used for calculating drainage basin orientation (a),
847 sinuosity of main drainage (Smd), crescentness index (c), and sinuosity of anticline divide (d).

848 Fig. 8. Map of the 57 drainage basins and their main channel networks with respect to the three
849 zones. Red arrows depict the asymmetry directions of the drainage basins.

850 Fig. 9. Box plots showing the distribution of Ba (km^2), S (%), Bs, HI, AF, CI, Smd, and
851 DBO in three zones of the study area. Box plots represent 25–75% of values, the caps at the
852 end of the vertical lines represent 10–90% of values and the line in the center of the box
853 shows the median value.

854 Fig. 10. Box plots showing the distribution of Ba (km^2), S (%), Bs, HI, AF, CI, Smd, and
855 DBO in the northern and southern limbs of the Handun anticline.

856 Fig. 11. Schematic illustration of the formation of asymmetric forked drainage pattern or
857 curved drainage in a crescent-shaped basin, due to the lateral growth of a fold. With further
858 lateral anticline growth, the general trend of the main channel of the crescent-shaped drainage
859 basin becomes oblique to the fold axis, resulting in an increased value of drainage basin
860 orientation (DBO).

861 Fig. 12. Oblique fractures oriented oblique to the anticline axis having a major control in the
862 increase of drainage basin orientation in basins 10, 16, 18, and 19.

863 Fig. 13. Schematic representation of the joining of oblique fault/fracture to the normal
864 fault/fracture oriented parallel to the fold axis. At first stage, a drainage coinciding with an
865 oblique fault/fracture is developed (a). With progressive erosion and growth of the anticline
866 over time (b), the oblique drainage can join to the drainage coinciding with the trace of normal
867 fault/fracture oriented parallel to the fold axis, and thereby a curved drainage with high DBO
868 is formed.

869 Fig. 14. Dendritic, parallel, curved parallel, asymmetric forked, fan-shaped, radial, and semi-
870 annular drainage patterns developed on the flanks of the Handun anticline.

871

872 Table 1

Zone	Ba (km^2)	S (%)	Bs	HI	AF	CI	Smd	DBO	Sad	Dd	Dd1	Df
Western	1.93	23.25	5.34	0.63	15.31	1.09	1.19	22	1.23	5.91	3.32	9.28
Central	4.02	54.81	2.46	0.53	12.48	1.13	1.24	24.36	1.37	4.22	2.73	6.18
Eastern	1.73	31.33	4.58	0.46	5.53	1.04	1.16	13.67	1.03	5.01	3.31	6.93

873

874 Table 2

Parameter			Ba	S	Bs	HI	AF	CI	Smd	DBO
ANOVA test (Between Zones)			0.249	**0.000**	**0.000**	**0.000**	**0.011**	0.077	0.677	0.224
Tukey's post -hoc test	Zones to compare	1-2	0.242	**0.000**	**0.000**	**0.01**	0.432	0.275	0.726	0.823
		1-3	0.993	0.082	0.677	**0.000**	**0.009**	0.354	0.955	0.298
		2-3	0.488	**0.000**	0.093	0.162	0.129	0.072	0.733	0.201

875

876 Table3

Parameters	**Ba (km²)**	**S (%)**	**Bs**	**HI**	**AF**	**CI**	**Smd**	**DBO**	**Dd**	**Dd1**	**Df**
Northern limb	1.38	33.33	4.76	0.60	13.52	1.09	1.14	23.51	5.76	3.53	8.63
Southern limb	4.67	28.64	4.10	0.56	13.73	1.11	1.32	17.78	4.89	2.87	7.48

877

878 Table 4

	t-test parameters		
Parameters	T	df	Sig (2 tailed)
Ba	-2.103	17.82	**0.050**
S	1.045	55	0.300
Bs	0.947	55	0.334
HI	1.394	55	0.169
AF	-0.096	55	0.924
CI	-1.139	55	0.260
Smd	-2.040	17.903	0.056
DBO	1.603	55	0.115

879

880 Table 5

Basin No.	**Ba (km²)**	**S (%)**	**Bs**	**HI**	**AF (%)**	**CI**	**Smd**	**DBO**
1	0.15	8.54	6.16	0.67	10.66	1.00	1.07	19
2	0.16	10.20	4.81	0.59	26.28	1.01	1.07	23
3	0.17	18.23	3.63	0.51	19.95	1.04	1.14	19
4	0.75	11.37	5.96	0.71	15.76	1.31	1.20	32
5	0.41	20.68	4.87	0.74	18.86	1.02	1.07	12
6	0.16	21.20	9.38	0.60	25.45	1.01	1.04	7
7	0.11	18.87	11.43	0.66	10.54	1.02	1.03	6
8	0.39	18.30	5.38	0.70	13.25	1.03	1.04	18
9	0.37	22.36	5.39	0.55	10.45	1.01	1.07	12
10	0.77	24.54	2.47	0.67	21.66	1.07	1.06	22
11	0.33	19.45	4.70	0.68	18.83	1.01	1.05	13
12	0.24	18.34	6.72	0.71	19.88	1.03	1.06	15
13	0.22	17.37	6.89	0.73	10.91	1.01	1.05	14

14	0.20	18.62	6.73	0.73	7.39	1.04	1.05	21
15	0.59	28.97	3.05	0.57	12.48	1.08	1.14	17
16	1.97	31.10	2.23	0.69	25.08	1.10	1.11	32
17	0.86	18.87	7.82	0.77	15.36	1.09	1.15	27
18	2.37	24.38	6.17	0.54	18.85	1.14	1.24	36
19	2.21	26.66	5.71	0.57	7.61	1.14	1.32	38
20	3.82	22.88	7.48	0.48	7.06	1.14	1.27	41
21	3.11	25.95	5.83	0.55	15.30	1.04	1.15	30
22	6.66	32.91	3.41	0.58	35.23	1.09	1.19	38
23	3.71	34.49	5.12	0.69	17.94	1.15	1.18	32
24	2.16	35.17	8.03	0.65	6.45	1.12	1.18	42
25	3.19	42.91	3.25	0.66	4.87	1.07	1.25	20
26	2.24	49.93	3.85	0.72	9.31	1.10	1.18	20
27	1.05	43.82	4.14	0.62	5.33	1.06	1.11	23
28	1.13	51.64	2.42	0.62	5.53	1.09	1.25	5
29	0.65	50.02	4.09	0.59	11.17	1.07	1.05	27
30	0.66	54.18	2.75	0.50	7.92	1.06	1.04	0
31	1.71	48.05	1.16	0.53	0.81	1.23	1.14	10
32	0.29	42.58	5.24	0.47	5.02	1.07	1.15	26
33	0.66	57.85	1.92	0.57	18.83	1.03	1.25	29
34	0.57	69.27	1.53	0.51	9.15	1.14	1.14	28
35	0.78	66.79	1.41	0.54	16.69	1.34	1.16	38
36	1.04	64.86	1.41	0.43	22.35	1.14	1.11	29
37	4.86	57.79	1.42	0.47	10.47	1.15	1.43	42
38	2.85	42.56	8.94	0.44	4.00	1.06	1.17	45
39	0.42	28.26	2.62	0.45	4.46	1.02	1.11	9
40	0.06	24.63	2.79	0.41	1.46	1.01	1.17	7
41	0.33	23.05	4.03	0.47	16.35	1.01	1.18	6
42	0.92	21.85	3.73	0.51	3.99	1.03	1.10	5
43	5.78	47.65	5.37	0.50	2.94	1.11	1.22	10
44	14.92	52.89	1.65	0.48	26.08	1.13	1.64	18
45	25.74	57.71	1.40	0.43	26.11	1.23	1.79	46
46	4.47	38.01	2.24	0.72	19.88	1.16	1.37	7
47	2.31	38.13	5.39	0.68	6.07	1.07	1.11	3
48	3.38	27.01	3.32	0.73	13.87	1.02	1.09	14
49	2.80	24.12	4.95	0.64	23.31	1.09	1.24	18
50	2.96	23.57	6.94	0.56	4.80	1.18	1.25	27
51	10.52	26.06	1.71	0.41	24.02	1.25	1.37	41
52	5.97	24.01	2.33	0.61	16.70	1.31	2.57	43
53	0.69	20.00	4.87	0.65	16.85	1.05	1.13	13
54	0.73	23.02	3.87	0.68	10.01	1.07	1.11	13
55	2.13	20.75	3.31	0.52	7.85	1.28	1.41	35
56	0.18	13.06	8.21	0.61	17.33	1.02	1.03	12
57	0.25	9.99	7.77	0.52	9.52	1.02	1.04	2
Min	0.06	8.54	1.16	0.41	0.81	1.00	1.03	0.00
Mean	2.42	31.45	4.55	0.59	13.58	1.09	1.20	21.70
Max	25.74	69.27	11.43	0.77	35.23	1.34	2.57	46.00
SD	4.12	15.77	2.35	0.10	7.71	0.09	0.23	12.73

Table 6

Parameters	Ba	S	Bs	HI	AF	CI	Smd	DBO
Ba	1							
S	0.323*	1						
Bs	-0.32*	-0.573**	1					
HI	-0.314*	-0.363	0.305	1				
AF	0.344**	-0.094	-0.160	0.120	1			
CI	0.416**	0.329*	-0.374**	-0.185	0.077	1		
Smd	0.605**	0.177	-0.340**	-0.210	0.159	0.596**	1	
DBO	0.406**	0.226	-0.109	-0.202	0.232	0.593**	0.458**	1

** Significant correlation at the 0.01 level.

* Significant correlation at the 0.05 level.

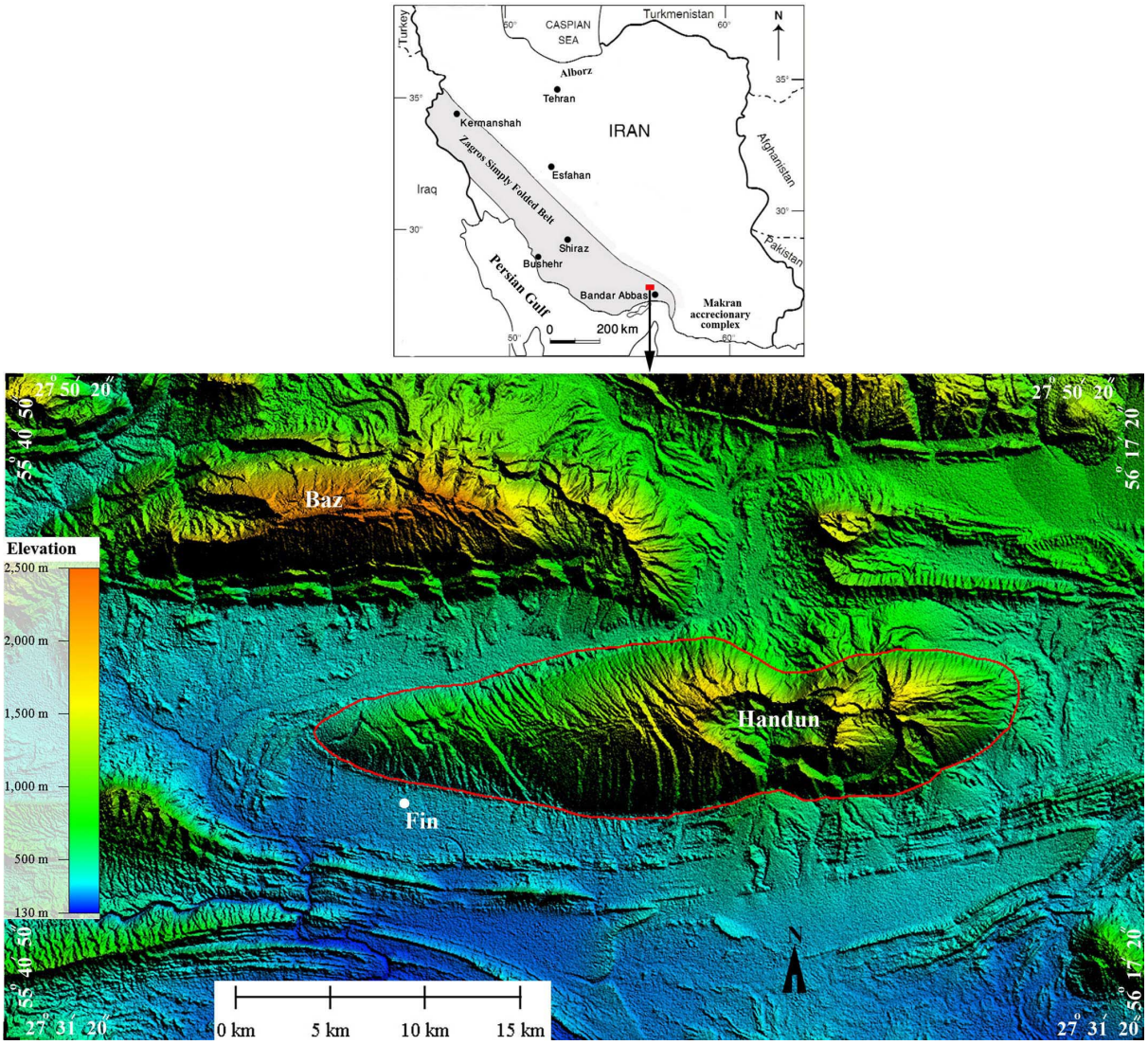
Turkmenistan
CASPIAN SEA
Turkey
Alborz
Tehran
Kermanshah
IRAN
Zagros Simply Folded Belt
Esfahan
Iraq
Afghanistan
Pakistan
Shiraz
Bushehr
Persian Gulf
Bandar Abbas
Makran accrecionary complex
0 200 km
N
Baz
Handun
Fin
Elevation
2,500 m
2,000 m
1,500 m
1,000 m
500 m
130 m
0 km 5 km 10 km 15 km

893

894 Fig. 1

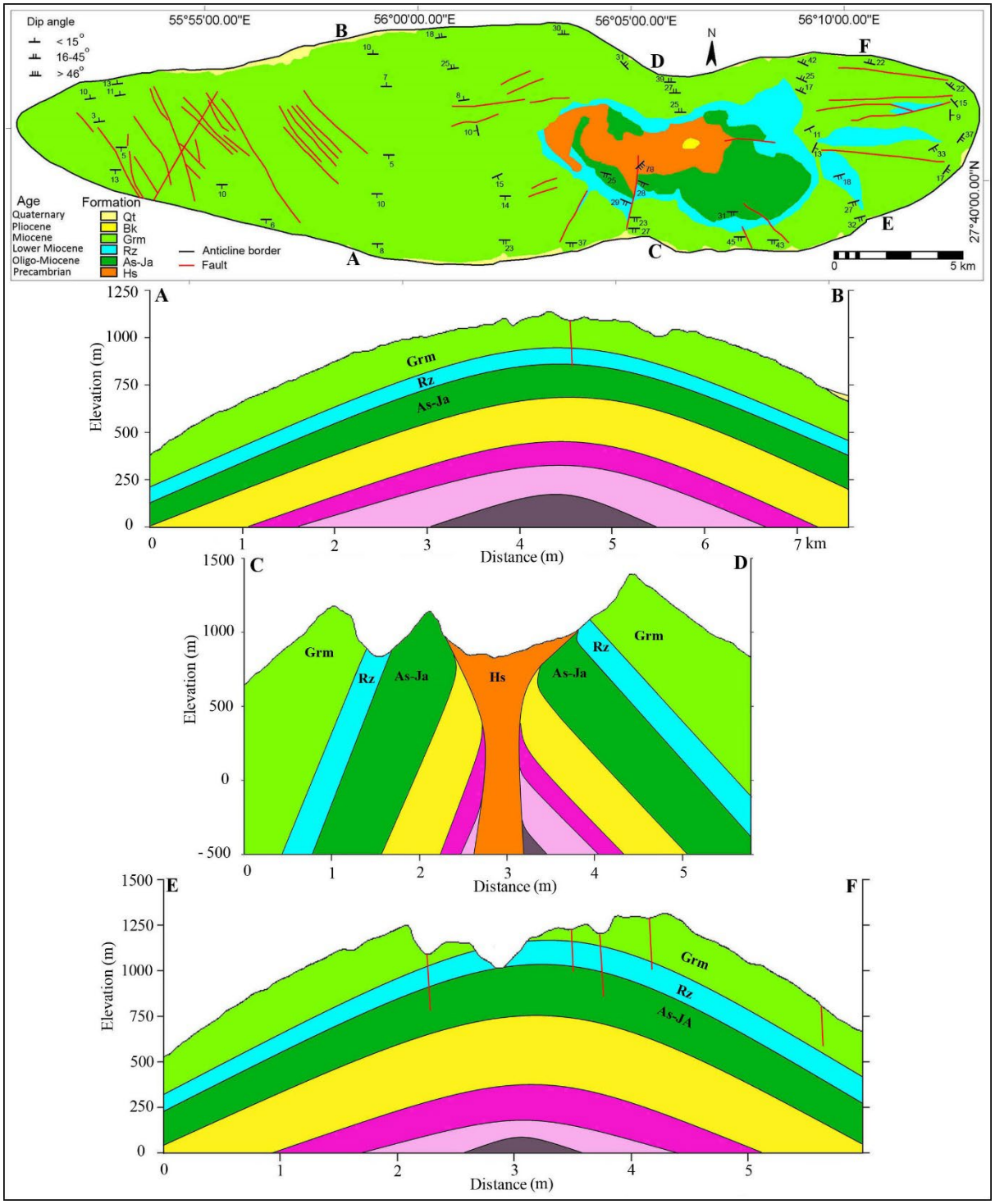
Dip angle
< 15°
16-45°
> 46°
55°55'00.00"E
56°00'00.00"E
56°05'00.00"E
56°10'00.00"E
27°40'00.00"N
N
A
B
C
D
E
F
Age
Formation
Quaternary
Pliocene
Miocene
Lower Miocene
Oligo-Miocene
Precambrian
Qt
Bk
Grm
Rz
As-Ja
Hs
Anticline border
Fault
0
5 km
Elevation (m)
Distance (m)
7 km
Grm
Rz
As-Ja
Hs
As-JA

Fig. 2

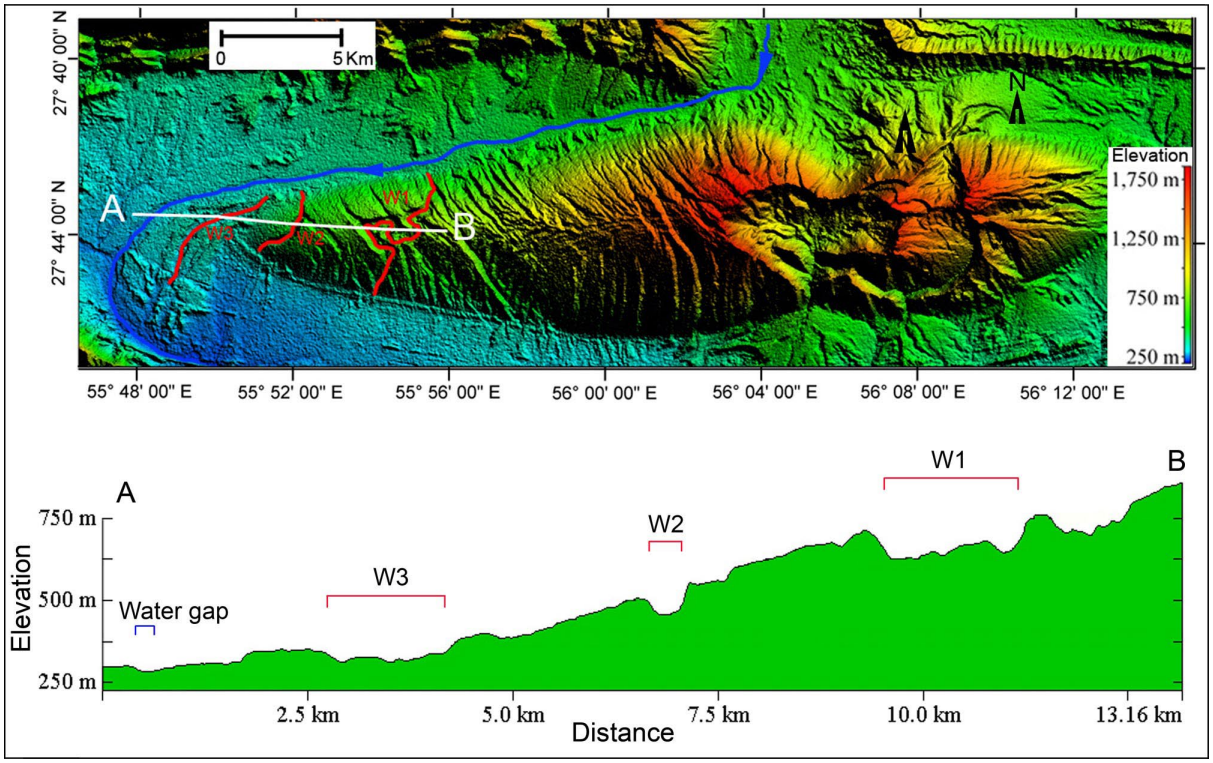
0
5 Km
N
Elevation
1,750 m
1,250 m
750 m
250 m
A
B
W1
W2
W3
27° 40' 00" N
27° 44' 00" N
55° 48' 00" E
55° 52' 00" E
55° 56' 00" E
56° 00' 00" E
56° 04' 00" E
56° 08' 00" E
56° 12' 00" E
A
B
W1
W2
W3
Water gap
750 m
500 m
250 m
Elevation
2.5 km
5.0 km
7.5 km
10.0 km
13.16 km
Distance

Fig. 3

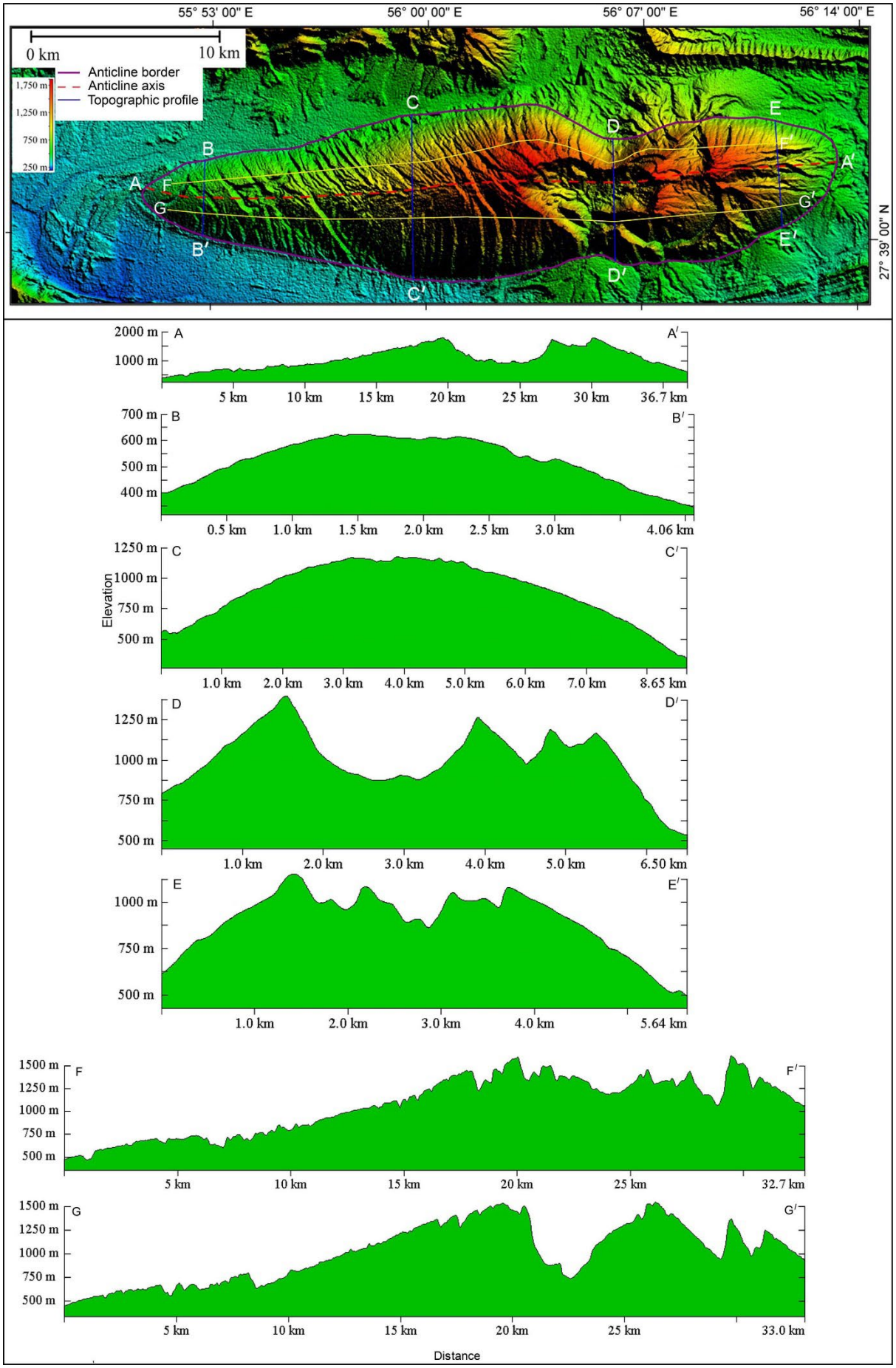
55° 53' 00" E
56° 00' 00" E
56° 07' 00" E
56° 14' 00" E
27° 39' 00" N
0 km
10 km
Anticline border
Anticline axis
Topographic profile
1,750 m
1,250 m
750 m
250 m
N
A
A′
B
B′
C
C′
D
D′
E
E′
F
F′
G
G′
Elevation
Distance
2000 m
1000 m
5 km
10 km
15 km
20 km
25 km
30 km
36.7 km
700 m
600 m
500 m
400 m
0.5 km
1.0 km
1.5 km
2.0 km
2.5 km
3.0 km
4.06 km
1250 m
1000 m
750 m
500 m
1.0 km
2.0 km
3.0 km
4.0 km
5.0 km
6.0 km
7.0 km
8.65 km
6.50 km
5.64 km
1500 m
32.7 km
33.0 km

900

901 Fig. 4

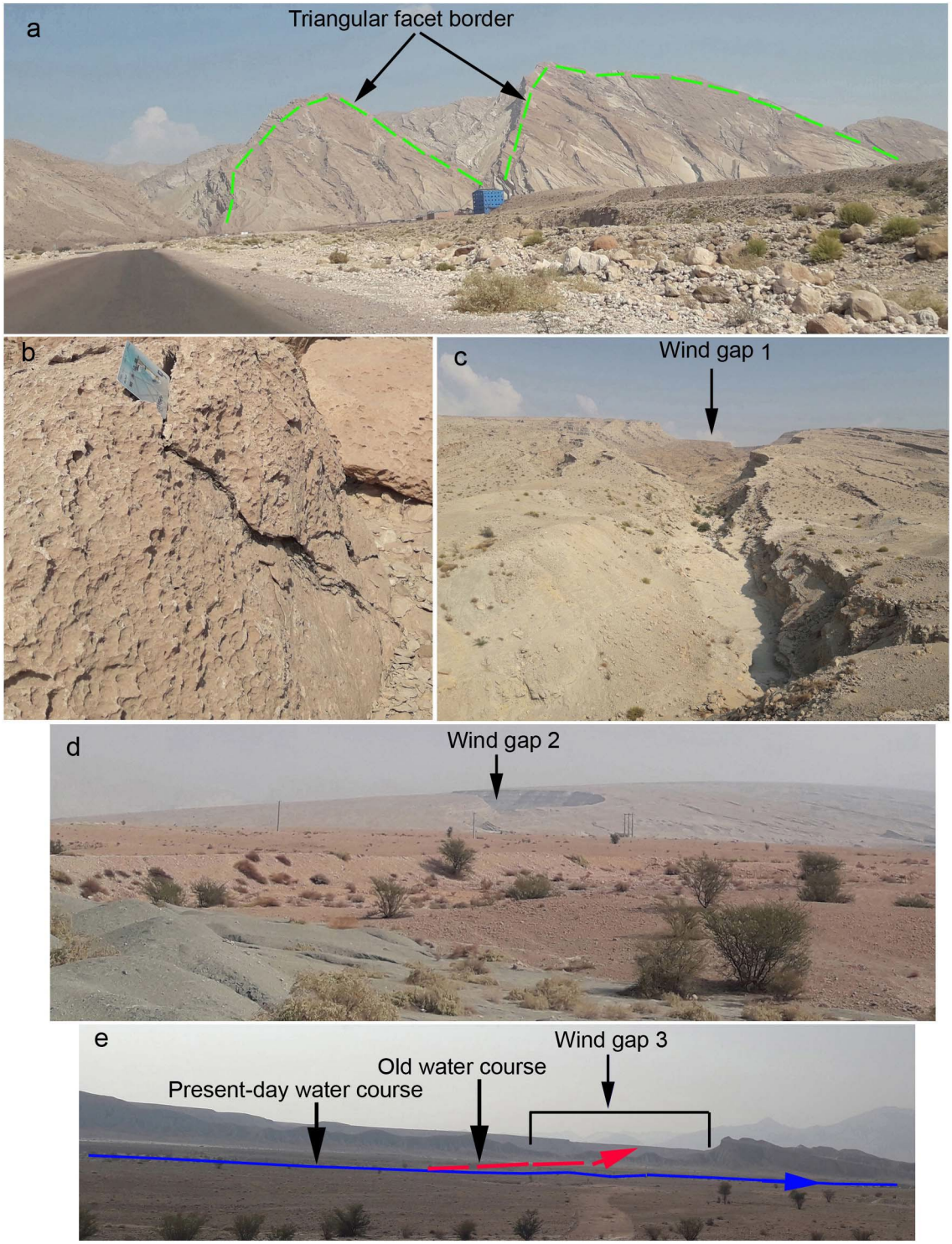

902

903 Fig. 5

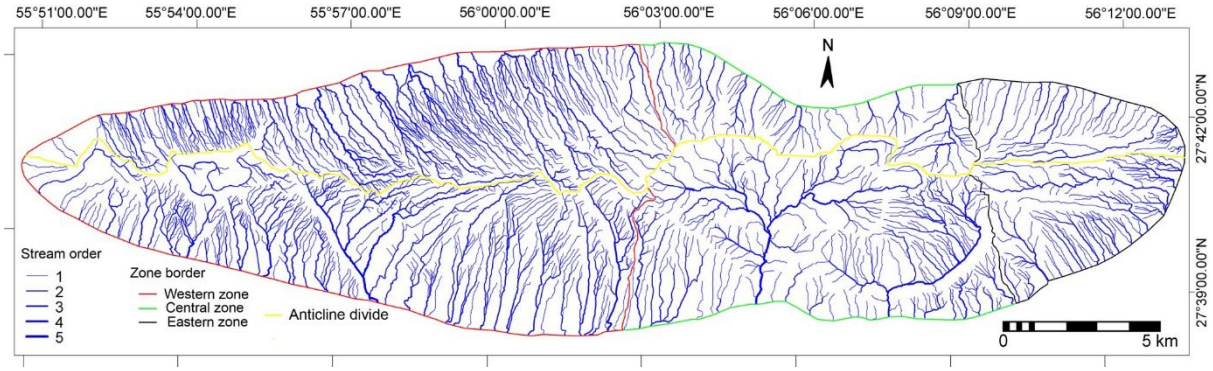

904

905 Fig. 6

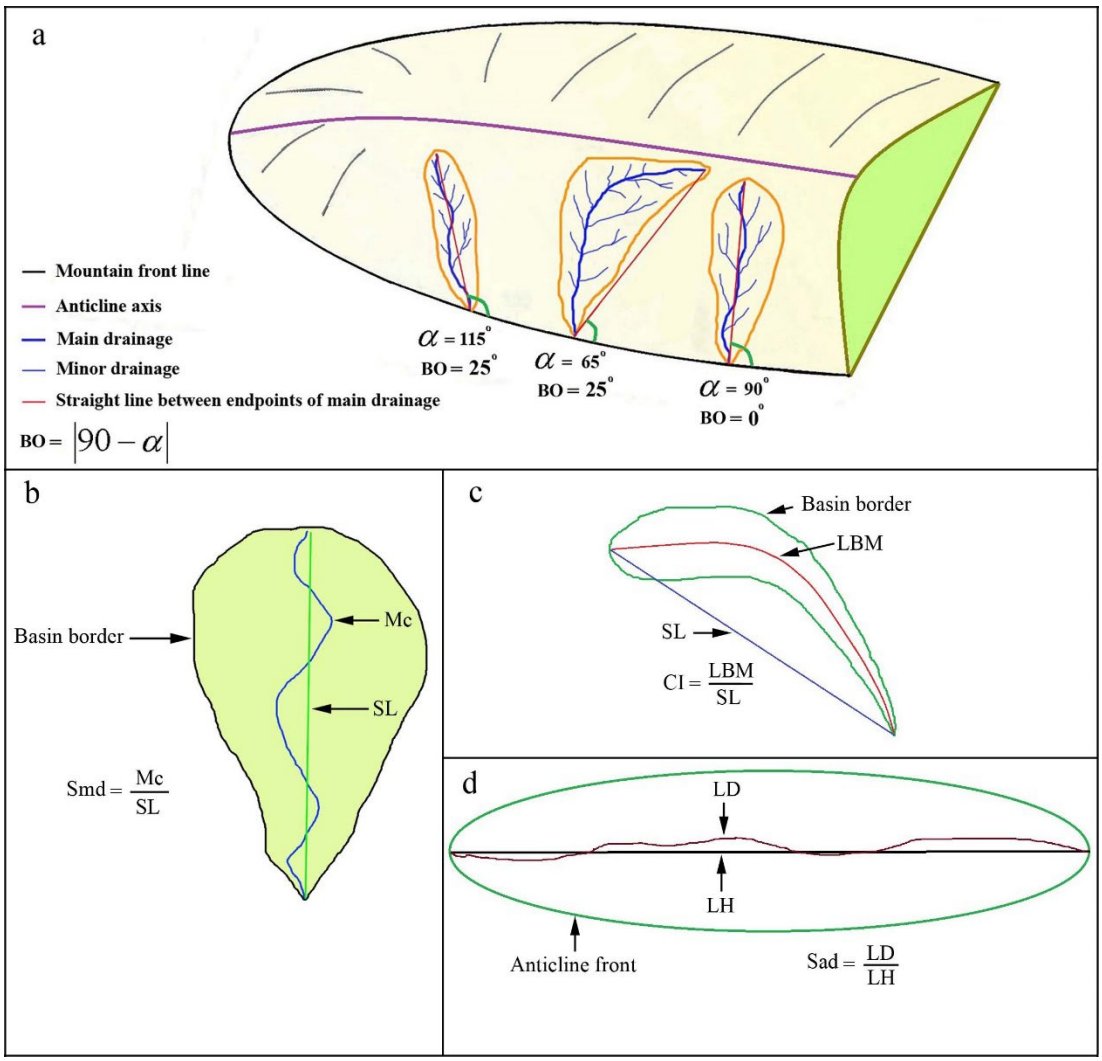

906

907 Fig. 7

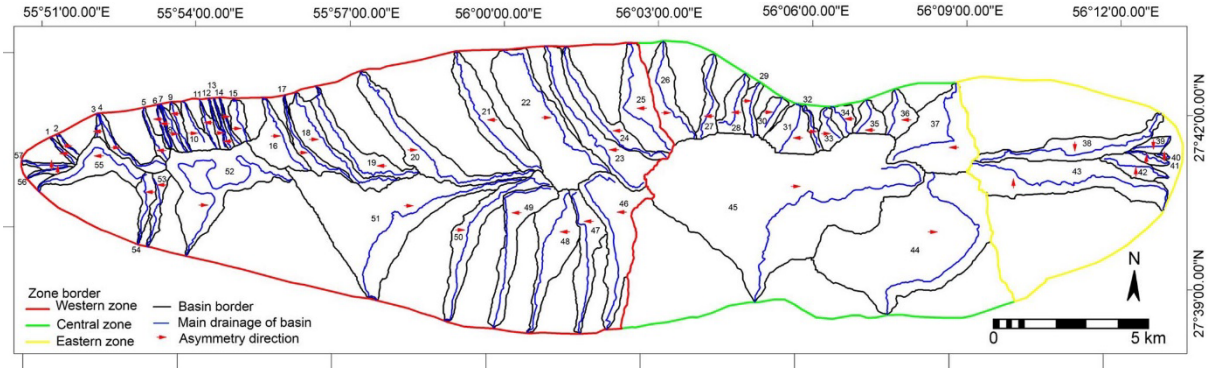
55°51'00.00"E
55°54'00.00"E
55°57'00.00"E
56°00'00.00"E
56°03'00.00"E
56°06'00.00"E
56°09'00.00"E
56°12'00.00"E
27°42'00.00"N
27°39'00.00"N
Zone border
Western zone
Central zone
Eastern zone
Basin border
Main drainage of basin
Asymmetry direction
N
0
5 km

908

909 Fig. 8

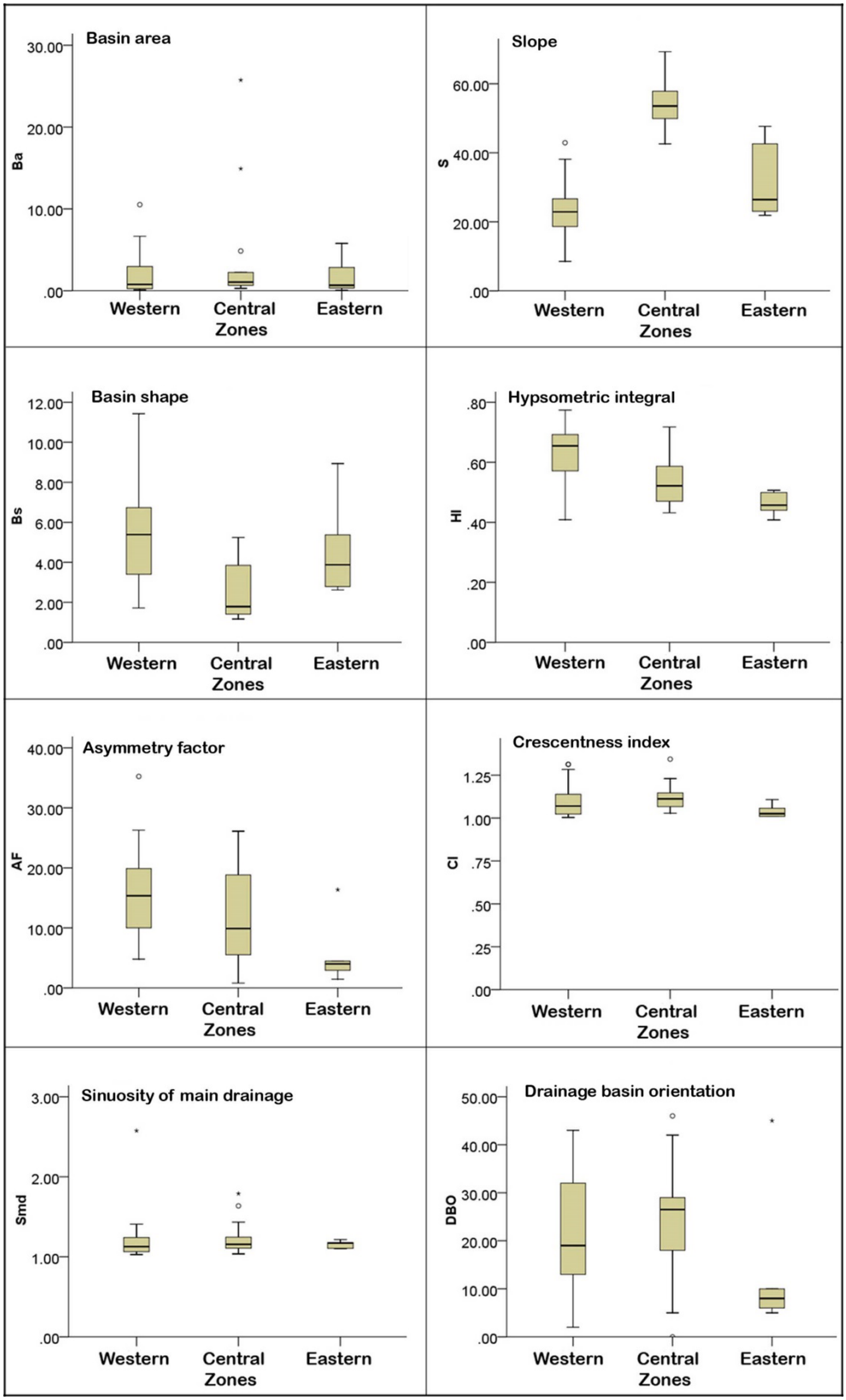
Basin area
Ba
30.00
20.00
10.00
.00
Western
Central
Zones
Eastern
Slope
S
60.00
40.00
20.00
.00
Western
Central
Zones
Eastern
Basin shape
Bs
12.00
10.00
8.00
6.00
4.00
2.00
.00
Western
Central
Zones
Eastern
Hypsometric integral
HI
.80
.60
.40
.20
.00
Western
Central
Zones
Eastern
Asymmetry factor
AF
40.00
30.00
20.00
10.00
.00
Western
Central
Zones
Eastern
Crescentness index
CI
1.25
1.00
.75
.50
.25
.00
Western
Central
Zones
Eastern
Sinuosity of main drainage
Smd
3.00
2.00
1.00
.00
Western
Central
Zones
Eastern
Drainage basin orientation
DBO
50.00
40.00
30.00
20.00
10.00
.00
Western
Central
Zones
Eastern

910

911 Fig. 9

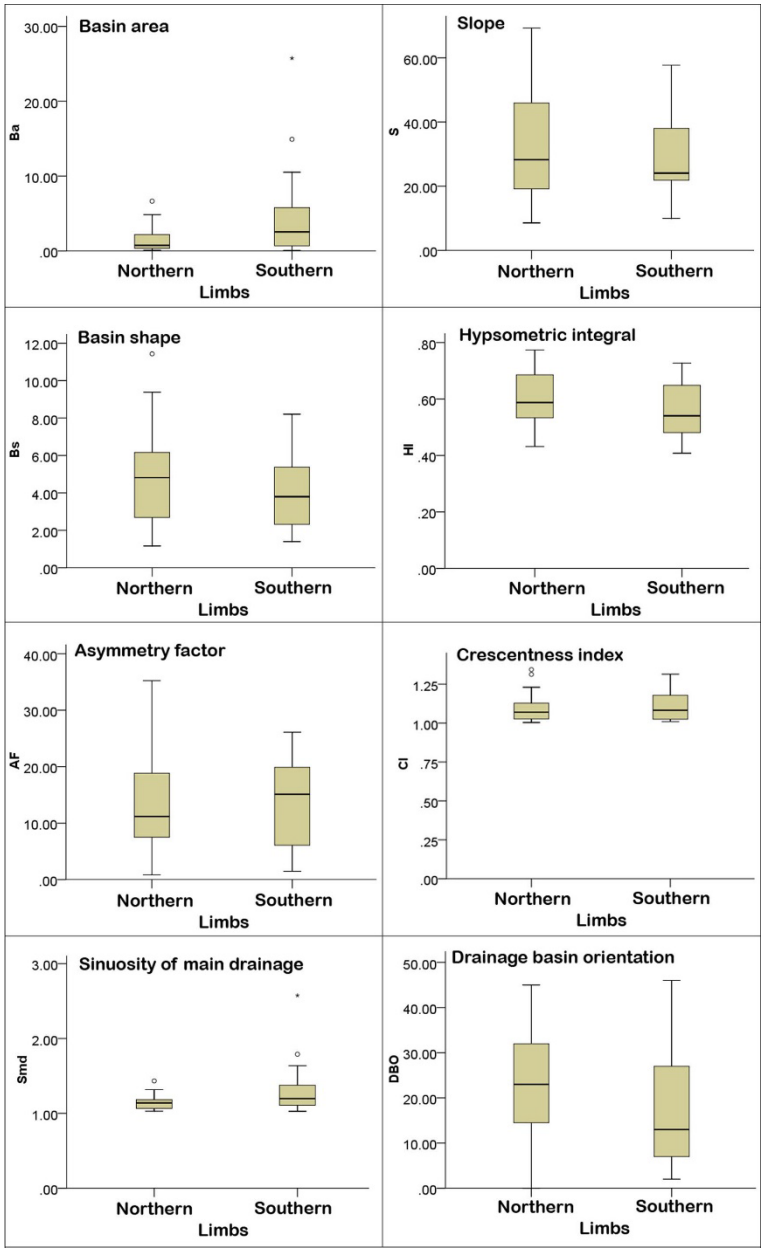

912

913 Fig. 10

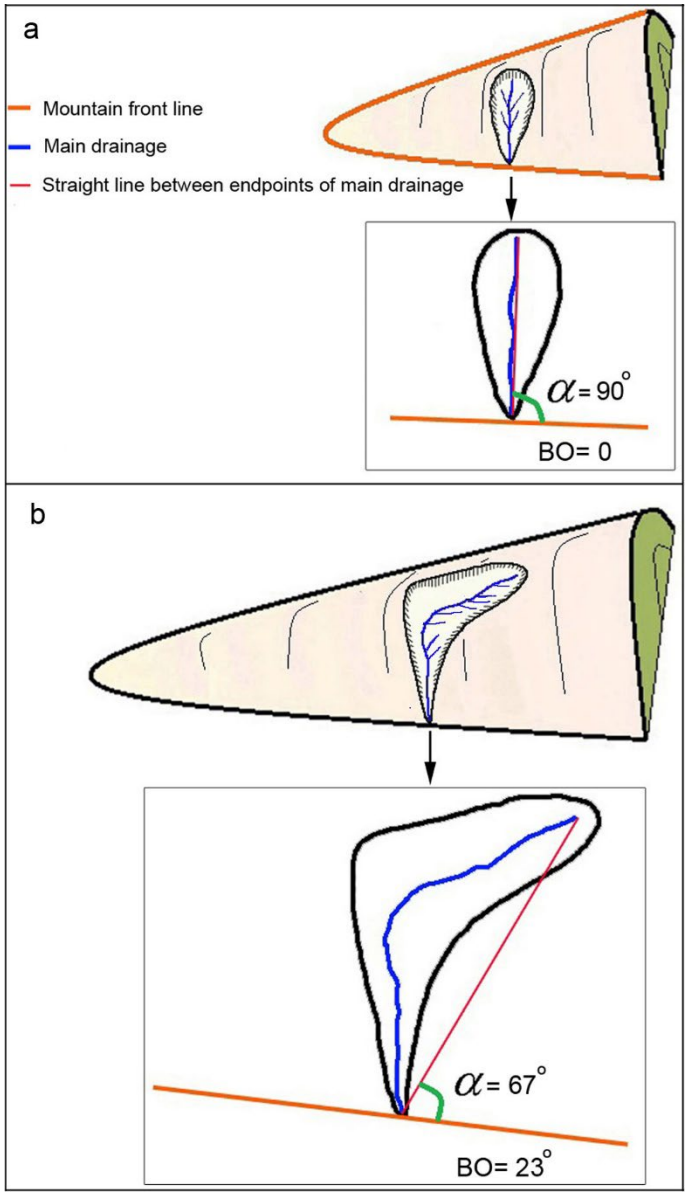

914

915 Fig. 11

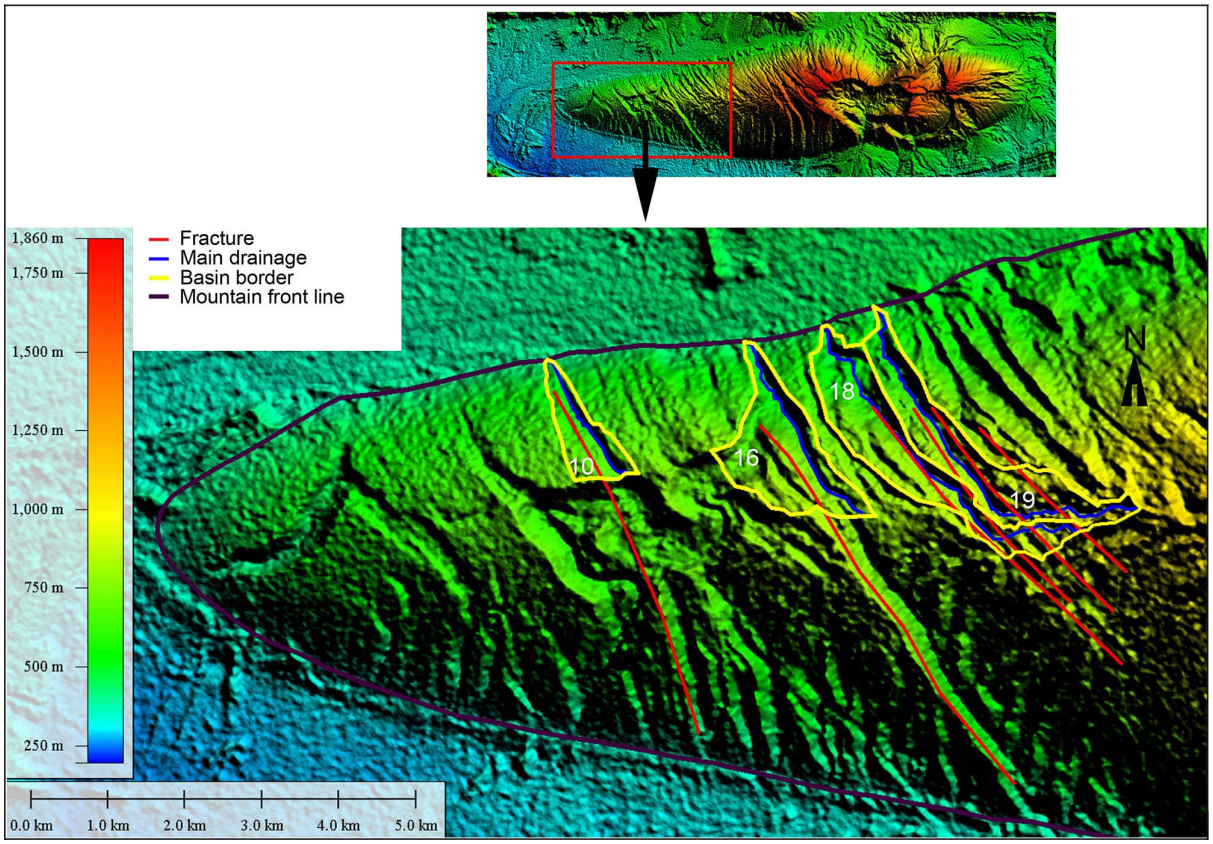

916

917 Fig. 12

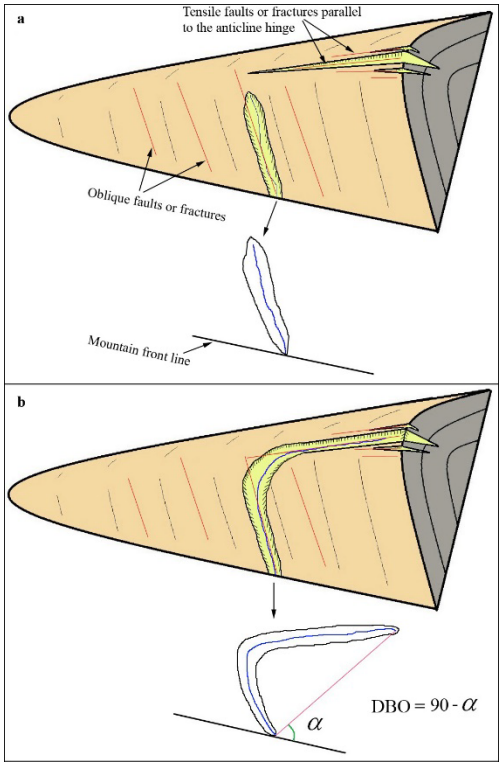

918

919 Fig. 13

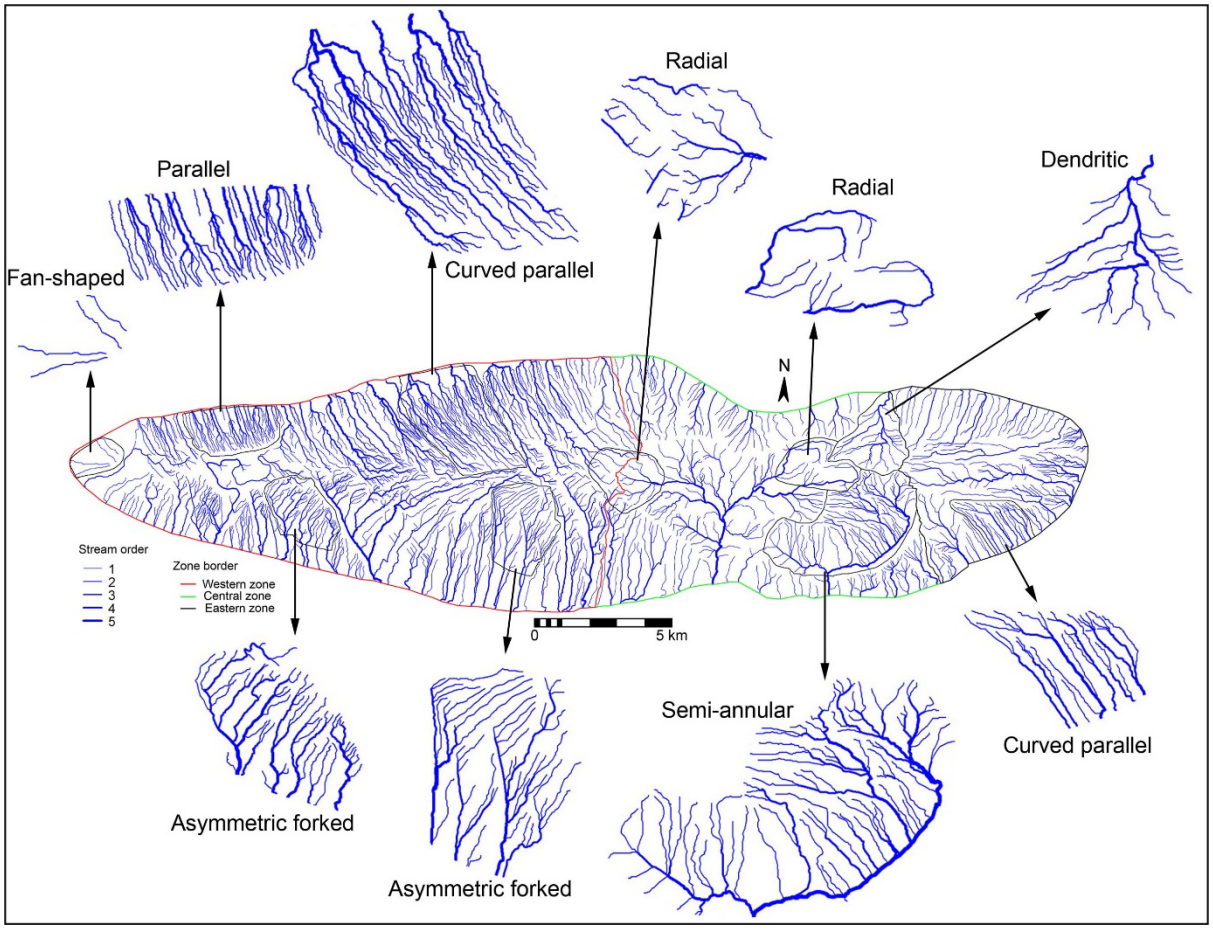
Radial
Parallel
Dendritic
Radial
Fan-shaped
Curved parallel
N
Stream order
1
2
3
4
5
Zone border
Western zone
Central zone
Eastern zone
0
5 km
Asymmetric forked
Semi-annular
Curved parallel
Asymmetric forked

Fig. 14